


# Analysis of a Temperature-Controlled Exhaust Thermoelectric Generator During a Driving Cycle

F.P. BRITO <sup>1,4</sup> A. ALVES,<sup>1</sup> J.M. PIRES,<sup>1</sup> L.B. MARTINS,<sup>1</sup> J. MARTINS,<sup>1</sup> J. OLIVEIRA,<sup>1</sup> J. TEIXEIRA,<sup>1</sup> L.M. GONCALVES,<sup>2</sup> and M.J. HALL<sup>3</sup>

1.—Mechanical Engineering Department, Universidade do Minho, Campus de Azurém, 4800-058 Guimaraes, Portugal. 2.—Industrial Electronics Department, Universidade do Minho, Campus de Azurém, 4800-058 Guimaraes, Portugal. 3.—Department of Mechanical Engineering, University of Texas at Austin, Austin, TX, USA. 4.—e-mail: francisco@dem.uminho.pt

Thermoelectric generators can be used in automotive exhaust energy recovery. As car engines operate under wide variable loads, it is a challenge to design a system for operating efficiently under these variable conditions. This means being able to avoid excessive thermal dilution under low engine loads and being able to operate under high load, high temperature events without the need to deflect the exhaust gases with bypass systems. The authors have previously proposed a thermoelectric generator (TEG) concept with temperature control based on the operating principle of the variable conductance heat pipe/thermosiphon. This strategy allows the TEG modules' hot face to work under constant, optimized temperature. The variable engine load will only affect the number of modules exposed to the heat source, not the heat transfer temperature. This prevents module overheating under high engine loads and avoids thermal dilution under low engine loads. The present work assesses the merit of the aforementioned approach by analysing the generator output during driving cycles simulated with an energy model of a light vehicle. For the baseline evaporator and condenser configuration, the driving cycle averaged electrical power outputs were approximately 320 W and 550 W for the type-approval Worldwide harmonized light vehicles test procedure Class 3 driving cycle and for a real-world highway driving cycle, respectively.

**Key words:** Thermoelectric generator, exhaust heat recovery, heat exchanger model, variable conductance heat pipes, thermosiphon, driving cycles, automotive heat recovery

## Nomenclature

1D	One-dimensional	ICE	Internal combustion engine
3D	Three-dimensional	IMEP	Indicated mean effective pressure
ATDC	After top dead centre	LaMoTA	Laboratory of thermal engines and applied thermodynamics
BMEP	Brake mean effective pressure	MBT	Maximum brake torque
BSFC	Brake specific fuel consumption	MEP	Mean effective pressure
CFD	Computational fluid dynamics	NEDC	New European driving cycle
EGR	Exhaust gas recirculation	NTU	Number of transfer units
EVO	Exhaust valve opening	OEM	Original equipment manufacturer
FMEP	Friction mean effective pressure	PMEP	Pumping mean effective pressure
GPS	Global positioning system	TE	Thermoelectric
HP	Heat pipe	TEG	Thermoelectric Generator
HW	Highway driving cycle	VHCP	Variable conductance heat pipe
IC	Internal combustion	VSP	Vehicle specific power
		WLTP	Worldwide harmonized light vehicles test procedure
		WOT	Wide open throttle

(Received June 16, 2015; accepted November 17, 2015; published online December 11, 2015)

**Variables**

$c_{p \text{ exh}}$	Exhaust specific heat at constant pressure [W/(mK)]
$A_{\text{avg}}$	Reference section area (m <sup>2</sup> )
$A_{\text{fins}}$	Total area of the fins (m <sup>2</sup> )
$A_{\text{no fins}}$	Total outer tube area excluding fin area (m <sup>2</sup> )
$A_{\text{wall out}}$	Outer wall surface area (m)
$Bi_{\text{boil}}$	Boiling Biot number
$Bi_{\text{conv}}$	Convection Biot number
$C$	Constant used in Eq. 3
$D_{\text{ext}}$	External tube diameter (m)
$Fo$	Fourier number
$h_{\text{boil}}$	Boiling heat transfer coefficient [W/(m <sup>2</sup> K)]
$h_{\text{conv}}$	Convection heat transfer coefficient [W/(m <sup>2</sup> K)]
$h_{\text{conv corr}}$	Corrected convective heat transfer coefficient [W/(m <sup>2</sup> K)]
$i$	Index of spatial node located at a depth $x$ from the outer surface of the tubes
$k_f$	Thermal conductivity of the fluid [W/(mK)]
$k_{\text{metal}}$	Tube thermal conductivity [W/(mK)]
$L_{\text{cond}}$	Active length of the condenser (m)
$L_{\text{cond max}}$	Full length of the condenser (m <sup>2</sup> )
$\text{Load}_{\text{cond}}$	Condenser Load (%)
$m$	Index of instant $t$
$\dot{m}_{\text{exh}}$	Exhaust mass flow rate (kg/s)
$n$	Constant used in Eq. 3
$N$	Number of tube rows (longitudinally)
$p$	Pressure (MPa) as used in Eq. 4
$P_{\text{avail}}$	Available (absorbable) exhaust power (W)
$P_{\text{cond}}$	Thermal power absorbed by the condenser (W)
$P_e$	Electric power produced by the thermoelectric modules (W)
$P_{\text{evap}}$	Evaporator thermal power (boiling) (W)
$P_{\text{exh}}$	Thermal power released by the exhaust air to the system (W)
$P_{\text{ICE}}$	Instantaneous engine propulsion power (W)
$P_{\text{Prop}}$	Instantaneous vehicle propulsion power (at the wheels) (W)
$Pr$	Prandtl number
$Pr_w$	Prandtl number evaluated at wall surface temperature
$P_{\text{wall out}}$	Thermal power absorbed from exhaust gases at outer evaporator wall surface (W)
$Re_{d,\text{max}}$	Reynolds number based on the maximum velocity achieved at the smallest cross section area of the tube banks
$S_n$	Transversal pitch between evaporator tubes (m)
$S_p$	Longitudinal pitch between evaporator tubes (m)
$T_{\text{exh avg}}$	Average Exhaust temperature (°C)

$T_{\text{exh in}}$	Exhaust inlet temperature (°C)
$T_{\text{exh out}}$	Exhaust outlet temperature (°C)
$T_{\text{hp}}$	Temperature of the boiling water inside the tube (°C)
$T_{\text{wall in}}$	Inner evaporator wall surface temperature (°C)
$T_{\text{wall out}}$	Outer evaporator wall surface temperature (°C)
$u_{\text{max}}$	Maximum fluid velocity (m/s)
$\alpha$	Material diffusivity (m <sup>2</sup> /s)
$\Delta T$	Temperature difference (°C)
$\Delta T_{\text{log}}$	Mean logarithmic temperature difference (°C)
$\Delta t$	Time step used in evaporator model (s)
$\Delta x$	Space step used in evaporator model (ms)

## INTRODUCTION

### Vehicle Efficiency Improvement

Increasingly stringent efficiency and emissions standards imposed on road vehicles are requiring the automotive industry to find new ways to comply with these demands. The improvement of energy efficiency and emissions may be achieved by reducing the primary energy consumption of the vehicle through the use of intrinsically cleaner, higher efficiency engines, the use of vehicle hybridization and also by recovering some of the energy that is normally wasted by the vehicle.

Growing vehicle electrification and powertrain hybridization allows reducing many of the aforementioned problems. This could mean the use, to a higher degree, of more efficient electric-driven components (e.g. pumps, motors and drives, air conditioning systems), the regeneration of some of the braking energy or the employment of electric propulsion in the situations where ICEs are less effective, namely under low loads and vehicle motion starts.<sup>1,2</sup>

### Exhaust Waste Heat Recovery

Nevertheless, engines still waste, through the tailpipe, about the same amount of thermal power they produce mechanically, even when operating at top efficiency.<sup>3,4</sup> It is therefore advantageous to recover a portion of this wasted energy by converting it into electricity.<sup>5</sup> This electric recovery will be especially useful in the case of vehicles having a high degree of electrification, synergistically increasing the efficiency potential.

### TEGs

The use of Seebeck effect thermoelectric generators (TEGs) for the electric recovery of exhaust enthalpy<sup>5,6</sup> is one of the few methods for directly converting thermal energy into electric energy

without the need for moving parts or mechanically complex systems as in the case of the systems based on the Rankine Cycle. Their simplicity constitutes their main advantage. However, there are still some obstacles for their widespread use in heat recovery. Current commercially available Thermoelectric (TE) modules typically display a low power density (due to their typically low efficiency), have high cost per unit of generated power and require complex thermal management to operate efficiently under variable thermal load.<sup>7</sup>

The power density and cost of new modules is steadily improving. The exploration of phenomena such as quantum confinement and the use of techniques such as material nanostructuring is allowing the development of new materials with improved properties (namely, regarding the maximization of the Seebeck coefficient and the minimization of the electric resistivity and thermal conductivity).<sup>6,8</sup> This allows the reduced usage of rare earth materials such as tellurium, substituting these with other relatively abundant raw materials.

Module cost may also be diminished by reducing raw material usage. It has been proved that the optimal TE pellet thickness for maximum electric power could be significantly reduced if the thermal resistances upstream and downstream of the thermoelectric junctions (namely those related to contact resistances) could be minimized.<sup>9</sup> This would result in a higher thermal power usage by the modules, and also in a net gain in total electric power produced, provided there would be sufficient heat available. The authors have been exploring this strategy in recent research.<sup>10</sup>

### Thermal Management Challenges: Variable Engine Load

One of the biggest challenges for automotive TEGs is their thermal management. This is due, on one hand, to their temperature limitations, and on the other hand, to the strong dependency of output on the temperature differential ( $\Delta T$ ) across the TE junctions.<sup>9</sup> For fixed physical properties, this electric power output varies with the square of  $\Delta T$ . Therefore, the temperature at the hot junctions of the module should be as high as possible, but not so high as to exceed their temperature limit. This fine temperature tuning can be done under fixed operating conditions, but it is a challenge to attain under variable exhaust power, as in the case of a vehicle performing a driving cycle.

Ideally, the generator's heat exchangers should be able to adapt to the broadest possible range of engine loads during the driving cycle, displaying a low thermal resistance enabling the generator to produce electricity even under medium to low exhaust power events. Nonetheless, the system should prevent any temperature overshoots under high power events. It should be a system with enough installed power (e.g. high number of TE

modules) in order to take full advantage of high exhaust power events, while still avoiding excessive thermal dilution under low to medium exhaust power events. To the best of the authors' knowledge, the thermal management required to conform to these specifications has not been made until now.

There are several examples of OEM-backed projects for the automotive exhaust thermoelectric generators.<sup>11,12,13</sup> TEG prototypes are normally optimized for a given exhaust load, operating sub-optimally under lower loads (due to thermal dilution) and needing to reject the extra thermal energy under higher power events through the use of bypass systems to avoid module overheating. Heat transfer methods generally rely on passive convective (e.g. finned surfaces) and conductive (through solid materials) heat transfer methods to capture exhaust heat. In this way, it is not easy to control both the thermal power and the temperature obtained during variable load operation. For instance, a low thermal resistance will be advantageous for maximizing heat absorption, but it will facilitate temperature overshoots under high thermal loads and vice versa.<sup>14</sup>

### Phase Change Thermo-Siphon Devices, Heat Pipes

It is possible to develop thermal management systems to avoid some of the aforementioned problems. One of the options would be to induce temperature uniformity on the substrate to which the modules are attached. This would equalize the hot face temperature, but it would also cause thermal dilution under low loads. The excessive thermal power reaching the system could also be modulated with a bypass system, but very hot gases could still be hot enough to harm the modules located within the first few rows in contact with the gases, even with reduced flow rates.

Another solution for thermal control is the use of an intermediate heat transfer medium between the exhaust flow and the modules, such as an oil flow circuit or a phase change device. These systems may allow the downgrading of excessive exhaust temperature and adapt, at least partially, to the thermal load. Thermo-siphon devices such as heat pipes (HP) and vapour chambers are good candidates. These devices transfer heat from a heat source to a heat sink with minimal thermal resistance, since they rely on the phase change principle. In the HP, a fluid entrapped within a closed space will cyclically absorb the heat at the heat source by vaporization and release it to the heat sink by condensation. The return of the fluid from the heat sink back to the heat source region is realized by gravity or by capillary effects in the presence of porous inner surfaces (e.g. wicked surfaces).<sup>15</sup>

At a first glance, it might seem illogical to incorporate an additional heat transfer process, with its inherent thermal resistance, into the

system. However, one big advantage will be obtained: if the inner pressure of this device can be controlled, then the heat transfer temperature can also be controlled. This will allow a precise temperature downgrade of the heat source for most of the engine load range. Conventional systems such as basic HPs vary their temperature according to thermal load, because there is no control over their inner pressure, which is related to the boiling temperature. Their inner pressure will depend on the amount of vaporized fluid present in its interior and on the rates of vaporization and condensation.<sup>15</sup> The ideal system would not significantly vary its temperature with load, so that the intended temperature would always be attained. Such a system would then vary its thermal load by changing its active heat transfer area instead. There are systems that operate similarly to this, such as the variable conductance heat pipe (VCHP).<sup>15</sup>

### Variable Load Heat Exchanger Concept and Advantages

A VCHP acts as an integrated evaporator/condenser in a single closed space, along with an expansion tank. It transfers the heat from the hot to the cold source by vaporizing a phase-changing fluid at the evaporator and then condensing it at the condenser. This concept may be applied to the present case by putting the evaporator heat exchanger into contact with the hot exhaust gases and putting the condenser heat exchanger into contact with the hot-side of the TE modules, as done in previous experimental work by the authors<sup>16</sup> (Fig. 1).

The VCHP utilizes a binary working fluid mixture consisting of a non-condensable gas (in this case air) combined with a condensable working fluid (in this case water). Under operation, a stratification of these species will take place and the volume occupied by each fluid will expand or contract according to the amount of each species present within the VCHP and their densities.

Under cold conditions, there will be little vapour present and the non-condensable gas will occupy most of the VCHP volume. Under operation, there will be vapour production, but the internal pressure increase due to vapour presence will be relatively small as the expansion tank is much larger than the VCHP volume. Under low thermal loads, there will be little vaporization and the non-condensable gas will occupy most of the HP volume, with the active condenser area having only a small fraction of condensable vapour. As the thermal load increases, the vapour will start to build-up, expanding and occupying an increasing fraction of the condenser and replacing and pushing the non-condensable gas out of the condenser area, into the expansion tank. While the two working fluids are not physically separated, under operation, the continuous vaporization of the phase change fluid occurs steadily enough so that the air is kept away from the evaporator area and a stratification of both fluids occur. This stratification can be observed by a stratification of the temperature along the height of the VCHP.<sup>16</sup> As thermal load increases, the active condenser area (and therefore the condensing power) will also increase. If the evaporative power drops below the condensing power, then the vapour mass will decrease and so will the active condenser power. This phenomenon provides the generator with a variable conductance effect. This means that, according to the thermal load at the hot source, a higher or a lower area/length of the condenser (heat sink) will be active, with the inactive part being occupied by the non-condensable gas. Under high loads, a higher amount of vapour produced will replace and push the non-condensable gas out of the condenser region, increasing its active length. Naturally, the amount of vapour present within the VCHP will depend not only on the vaporization rate, but also on the condensation rate.

The VCHP based evaporator/condenser concept may be adapted to a full size vehicle system with the condenser in contact with the hot-side of the thermoelectric modules. The cold side faces of the modules are attached to liquid or air cooled heat sinks. The authors have successfully tested this concept with a small Diesel engine and 12 off-the-shelf TE modules.<sup>16</sup> They succeeded in keeping a constant temperature at the hot face irrespective of engine load for several inner VCHP pressures. The maximum operating temperature of the modules (~250°C) was not tested, since the prototype was not prepared for the pressures that would be required to achieve it (around 40 bar using water). In fact, the main disadvantage of this system is the high pressures needed for boiling water at these temperature levels. Nevertheless, alternative phase change fluids could be used, such as Dowtherm-A, which boils at 250°C at pressures close to ambient.<sup>17</sup>

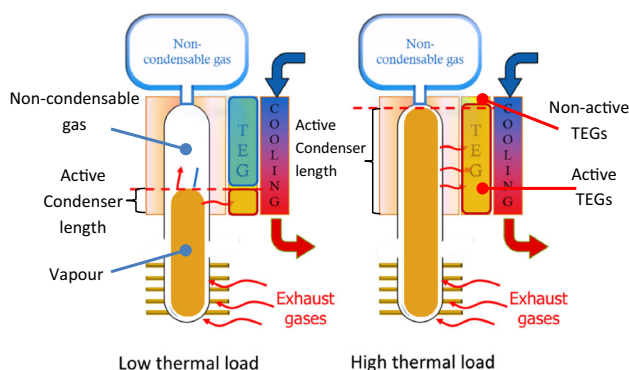


Fig. 1. Variable load thermoelectric generator concept based on a VCHP. Load varies through variation of active condenser length (TEGs are attached to heat sink of the VCHP).

## Exhaust Heat Exchangers

The heat exchangers used in exhaust systems require a sensible design, as they need to withstand temperatures that may exceed 800°C. At the same time, they should not induce too much back pressure as to affect engine performance. Exhaust gas recirculation (EGR) coolers are examples of widely used exhaust heat exchangers with an already optimized design. However, they are normally designed for a small fraction of the exhaust flow and for a heat sink temperature (the coolant circuit flow) around 90°C. TEG exhaust heat exchangers need to operate at higher heat sink temperatures (the target hot face module temperature is normally above 200°C and could be much higher) and channel the whole exhaust flow across it. Nonetheless, EGR coolers of big truck engines may be sufficient to allow full exhaust flow in smaller motorcar engines.

Several OEM-backed projects have proposed various heat exchanger designs,<sup>11,12,13</sup> normally based on finned exhaust ducts, which then transfer the heat to the modules through conduction. However, these systems do not easily control the temperature level attained at the hot face of the modules.

The design of a thermal energy recovery system from the exhaust gases based upon the VCHP concept involves the design and construction of two independent heat exchangers: one for the exhaust gas-thermosiphon (denoted as the evaporator) and another for the thermosiphon-TEG (denoted as the condenser). In each heat exchanger, the working fluid (in this case water) undergoes a phase change. The overall electrical energy recovered depends upon the heat that can be transferred from the exhaust gases to the TEG modules. If there are no losses to the environment, the evaporation and condensing heat transfer rates must eventually balance.

The condenser involves the transfer of heat from a phase change medium through a solid boundary and ultimately to the cooling fluid. The evaporator performance depends upon the heat transfer from the high temperature exhaust gases to the boiling water.

Because of the low thermal resistance of the phase change phenomena, it is the convective heat transfer (from the exhaust gases into the evaporator body) that effectively limits the overall performance of the unit. This results in different constraints for the two heat exchangers: the evaporator performance is limited by the available heat transfer area on the gas side which is critical due to system packaging. On the condenser side, the heat transfer medium is mostly condensed liquid which results in much greater convective heat transfer rates for a given heat exchanger surface area. At the cold side of the modules a good heat transfer medium (such as a liquid cooled heat sink) can be used to dissipate the heat from the TEGs to the environment, thus becoming less critical than the evaporator.

The most obvious design for a high inner pressure evaporator consists of finned tubes containing the phase change fluid, with the exhaust gases flowing outside of these tubes in cross flow. The analysis and design of the heat exchanger can be performed using a numerical CFD model. This has been successfully applied for analysis of fluid flow problems coupled with heat transfer, such as reported by Kumar.<sup>18</sup> The staggered tube bank heat exchanger geometry has already been extensively studied, with popular empirical correlations being available in the literature.<sup>14,17</sup> Given the wide range of physical phenomena involved that would render the complete model highly complex and difficult to optimize, in the present work, the empirical correlations for staggered tube bank heat exchanger design along with the Effectiveness-NTU method are used.<sup>14</sup> This will facilitate subsequent integration of sub models for the various components into a cohesive unit for energy recovery from waste heat. The details of the model are presented in subsequent sections.

## Engine Modelling

The exhaust heat exchanger model needs to receive, as an input, the instantaneous exhaust temperature and flow rate from an engine model. Traditionally there are three ways of evaluating engine performance: theoretical cycle analysis, modelling and experimental evaluation. Theoretical cycle analysis deals with the calculations of idealized thermodynamic cycles. It is very conjectural and is useful mainly to provide general performance trends.<sup>19</sup> Experimental evaluation is the best way to obtain engine data, but it involves having an actual engine at the test bench. Therefore, the most viable way to evaluate various data from a particular engine is to model it numerically. Numerical models are based on mathematical characteristics centred on physical and chemical modelling such as the ideal gas law, the first and second laws of thermodynamics, the physical properties of constituents and chemical properties required for combustion modelling.<sup>3,4</sup>

The overall engine is therefore modelled including combustion, heat transfer, fluid mechanics and dynamics, piston and valve position and velocities and global friction. There are several engine models on the market from companies such as RICARDO (Wave),<sup>20</sup> AVL (Boost),<sup>21</sup> FEV (Virtual engine),<sup>22</sup> Gamma Technologies (GT-POWER),<sup>23</sup> among others. The fluid flow and heat transfer within the engine interior can also be modelled with CFD codes such as KIVA,<sup>24</sup> ANSYS FLUENT<sup>25</sup> or CONVERGE,<sup>26</sup> but these are mainly used to calculate specific occurrences, as the CFD modelling would be exceedingly complex and time consuming for the overall evaluation of engine performance maps. The aforementioned numerical models can predict with very high accuracy values for power, efficiency, air

and fuel consumption, etc. Nevertheless, the increase in simulation detail normally also requires a proportionally higher degree of detail in the definition of the engine, which is not always easy to obtain. Also, many of the aforementioned commercial packages typically lack, for intellectual property security reasons, the degree of model transparency and configuration flexibility required for scientific work accountability. It is therefore frequent that research groups from the field of engine research choose to develop and use their own codes. Such was the choice of the authors, who have been using their own code for several years now.<sup>19,27,28</sup> This code, which has been refined over time,<sup>29</sup> is further summarized below. In the present work, this code is used for estimating several engine performance maps; namely, the torque, exhaust thermal power, temperature and flow rate as a function of engine load and speed.

The present engine model does not include after-treatment devices such as three-way catalysts. In real applications, the heat exchanger for the TEG system should be placed downstream of the three-way catalyst. The reactions occurring within these devices are globally exothermic,<sup>30</sup> but at the same time, there are also some thermal losses to the ambient along the exhaust pipe and the outer surface of the after-treatment system. Therefore, the authors decided to neglect the net effect of these phenomena within the overall model of the system, assuming that the outlet temperature of the exhaust gases will not differ from the generator inlet temperature by a meaningful amount.

### Energy Analysis of Driving Cycles

The simulation and evaluation of all the relevant energy flows involved in the running of a generic vehicle along a route in real-world driving conditions, is essential to the design of new powertrains for electric, hybrid electric or conventional ICE vehicles.

For this purpose, an energy model was developed and a code written in the MATLAB/Simulink environment that includes, in addition to the usual resistance forces, tyre longitudinal slip, cornering friction and road slope.<sup>31,32</sup> The study included the acquisition and processing of data obtained from a 5 Hz dedicated GPS. The collected pre-processed data includes time and space series of speed, altitude and curvature radius of the vehicle trajectory. The pre-processed real data, or the data from the type-approval tests (only a time series of the vehicle speed), was used as the input of the simulation model.

In the present work, the energy model is essential to obtain the time-load profile of the engine, and, via the engine model, the thermal load profile of the exhaust gases. The standard type-approval driving cycles are insufficient for this end, as they do not

include parameters that substantially affect the vehicle dynamics such as individual driving, road slope and additional friction due to cornering loads. In particular, several studies<sup>33–36</sup> based on the in-use fuel consumption data for European cars have concluded that the current type-approval cycle used in Europe, the New European Driving Cycle (NEDC), is unable to represent real-world driving conditions, as the certified test fuel consumptions are significantly lower than the corresponding average real data. One of the studies<sup>35</sup> showed that the deviation was higher than 60% for vehicles registered in 2012 and certified within the 90–100 gCO<sub>2</sub>/km bin.

The authors have recently proposed a methodology for the energy characterization of driving cycles, based on the numerical integration of specific power, including new parameters such as specific traction and braking energies, cumulative uphill and downhill slopes and cornering friction energy, as well as energy-power distributions.<sup>32</sup> The methodology is expected to help in the comparison of the available type-approval driving cycles and in the definition of more realistic ones that can be used for better assessment of fuel consumption and emissions of vehicles.

### Proposed Approach

The concept of a variable load, temperature controlled automotive exhaust TEG seems promising. However, there has not been any research assessing the merit of this concept under the variable conditions of a driving cycle. The present work aims to address this gap in the literature by performing a multidisciplinary analysis combining models for the energy analysis of driving cycles (e.g. computation of instantaneous traction power required), the engine (e.g. computation of exhaust gases temperature and flow rate maps) and a heat transfer model for the heat exchangers and thermoelectric modules (e.g. computation of thermal and electric powers). In the present work, the authors propose such an integrated model and explore it for a type-approval driving cycle (WLTP Class 3) and a recorded real Highway driving cycle performed by a small 1.6 L gasoline hatchback car.

## MODELLING

### Model Outline

An outline of the general approach used in the present work may be seen in Fig. 2. The driving cycle model estimates the instantaneous traction power and engine speed required to fulfil the specified driving cycle. The engine model then provides the exhaust gases mass flow rate and temperature for the conditions of the driving cycle. Finally, the thermoelectric generator model estimates the evaporator power, condenser power and

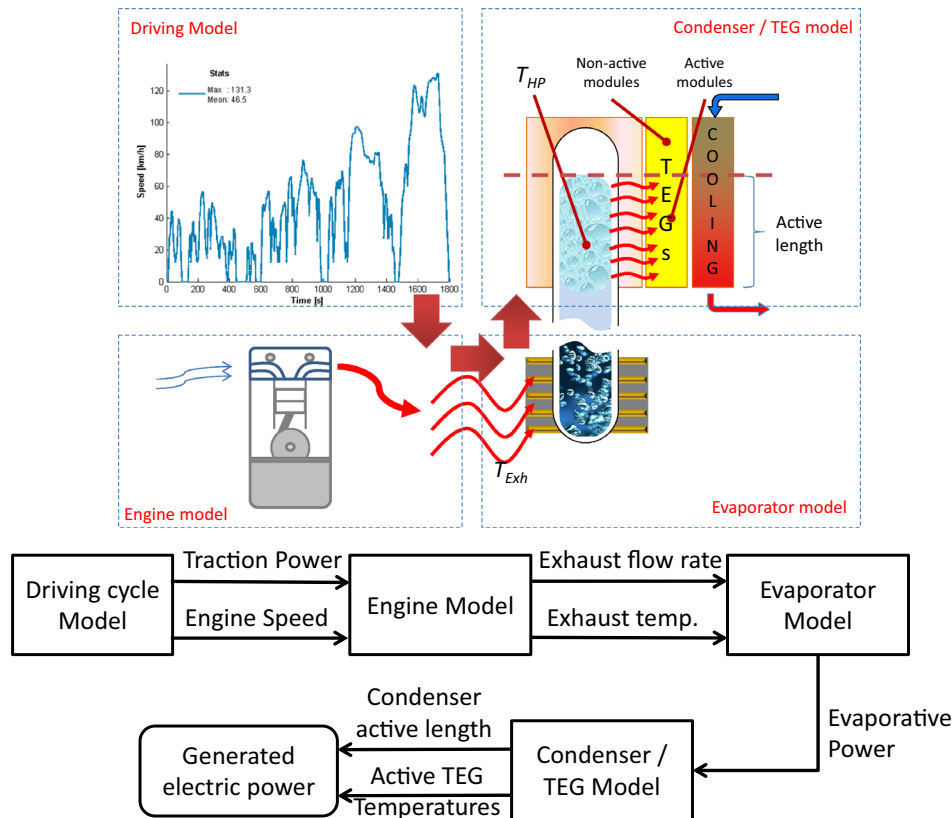


Fig. 2. Outline of the model overall structure, operation of heat fluxes between engine exhaust gases, evaporator and condenser and interaction between the several program modules.

electric power output for that driving cycle based on the input from the other models.

### Engine Map Characterization

The Laboratory of Thermal Engines (LaMoTA) of the Universidade do Minho developed an engine numerical model written in MatLab/SimuLink code to predict engine characteristics of normal Otto or Over-Expanded spark ignition engine cycles.<sup>27</sup> The program is a one zone model, with the combustion following a Wiebe function. It includes the Annand heat transfer coefficient,<sup>37</sup> where average constant temperatures are considered for the cylinder head, cylinder walls and piston. It includes a model for friction mean effective pressure.<sup>38,39</sup> Mass flow entering and leaving the cylinder is simulated using a compressible gas flow model.<sup>3</sup>

The model calculates the species inside the cylinder at any crank angle, as well as their temperature and pressure using the first law of thermodynamics. The properties (specific heat, ideal gas constant and the ratio of specific heats) of the different species are calculated from equations available in the literature.<sup>40,41</sup> Air is assumed to have the properties of an ideal gas. The gas exchange across the open valves is modelled using the compressible gas equation.<sup>3</sup>

The internal volume at each crank angle is calculated from the crankshaft and cylinder dimensions and the valve events are calculated from their

opening curves. The indicated work for each cylinder is calculated by integrating the pressure against volume along the 720° of the cycle. The indicated mean effective pressure (IMEP) is then obtained by dividing it by the swept volume. The brake mean effective pressure (BMEP) is obtained from IMEP and from the friction MEP<sup>4</sup>:

$$\text{BMEP} = \text{IMEP} - \text{FMPEP} \quad (1)$$

The combustion model (Wiebe function) incorporates two parameters which characterize the form factor and the combustion duration. Instead of using pre-imposed values, they were estimated within the program from load and rpm conditions using the analysis proposed by Bonatesta.<sup>42</sup>

The ignition timing is calculated iteratively to produce the maximum brake torque (MBT). Usually, to obtain MBT conditions, maximum pressure should occur near 10° after top dead centre (ATDC),<sup>3,4</sup> and in fact the model consistently predicts MBT conditions when maximum pressure occurs between 9° and 10° ATDC. An example of this may be seen in Fig. 3.

The engine model was run for the entire range of load (from closed throttle, with only mechanical and pumping losses, to wide open throttle—WOT) and speed (from 1000 rpm to 6000 rpm), and provided engine maps for torque, power, brake specific fuel

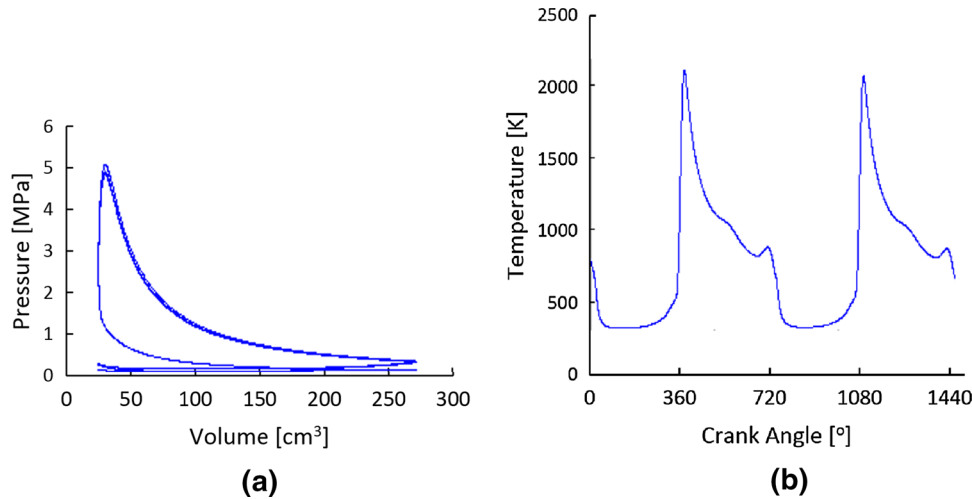


Fig. 3. Example of the engine model predictions during two consecutive engine cycles for (a) in-cylinder gas pressure as a function of the swept volume and (b) in-cylinder temperature as a function of crank angle.

consumption (BSFC), exhaust mass flow rate and exhaust temperature. Some of these maps are used together with the road model to obtain the instantaneous exhaust thermal power. The engine performance maps and indicators resulting from the modelling are presented in the upcoming Simulation Conditions section.

### Constant Temperature, Variable Load Heat Exchanger Concept Modelling

The concept of a constant temperature, variable load generator has already been explained above, and was used by the authors in previous work.<sup>16,43,44,45,46</sup> It relies on the application of a phase change device (e.g. a VCHP/thermosiphon) between the exhaust gases and the thermoelectric modules, which operates at nearly constant pressure and temperature. The thermal load variation during a driving cycle induces a variation in the active length of the condenser,  $L_{cond}$ , so that the condenser power will tend to match the evaporator power (recall Fig. 1). The maximum condenser power corresponds to the situation in which the whole length of the condenser is active,  $L_{cond} = L_{cond\_max}$ , that is, the whole length is occupied by vapour and none of it is occupied by air.

The load of the condenser may be defined as follows:

$$\text{Load}_{cond} = \frac{L_{cond}}{L_{cond\_max}} \quad (2)$$

If the evaporator power is lower than the maximum condenser power, this means there is not sufficient vapour being produced to occupy the whole length of the condenser and so it will operate at partial load ( $L_{cond} < L_{cond\_max}$ ) and only a fraction of the length will be active (only a fraction of the length will have condensation taking place). If

the evaporator power is greater than or equal to the maximum condenser power, this means there is sufficient vapour production to occupy the whole length of the condenser. Therefore, the condenser will be active along its entire length. It will be saturated (operating at full load) and there will be excess vapour production. This excess may be accumulated in the system up to a certain degree (although it will cause some pressure build-up) or it may be dissipated in an auxiliary condenser, as done experimentally in Ref. 16. The modelling of this system operation may be done similarly to<sup>16</sup> as follows:

- (a) The instantaneous evaporator power is calculated, ideally using a unsteady heat transfer model (the model used in Ref. 16 was used under steady state conditions).
- (b) The full load condenser power is calculated (power with the full length of the condenser being active).
- (c) If the instantaneous evaporator power is lower than the full load condenser power, then the active length of the condenser is corrected, until the condenser power matches the evaporator power. In a 1D thermal approach such as the present one, this will mean that all the heat transfer, temperature differentials and thermoelectric effects will occur solely along this active length. The active condenser and TE module area, as well as thermal resistances, will be reduced proportionally with the reduction of the active length (thermal resistance is inversely proportional to heat transfer cross-sectional area).
- (d) If the instantaneous evaporator power is higher than the full load condenser power, then the condenser will operate at full load and the condenser power will be calculated considering that condensation is occurring



along the full length of the condenser (the whole area of the modules is active).

- (e) The excess evaporator power may be considered as vapour accumulating within the volume of the system (i.e. as a kind of vapour buffer with a given capacity), or it may be considered to dissipate to the cooling system through an auxiliary condenser. If a vapour buffer is used, the vapour accumulated during excess evaporative power will be consumed during events in which the evaporator power is lower than the maximum condenser power.

With the aforementioned approach, the condenser load will be represented as the ratio between its active length and its total length according to Eq. 2. All main performance parameters will be roughly proportional to the condenser load, since the areas of all condenser layers, of modules attached to the condenser and of heat sinks attached to the modules, will also be proportional to the active length. The only term that might not be proportional to the active length is the condensation resistance, since the heat transfer coefficient obtained by the Nusselt theory for film condensation<sup>15,16</sup> also depends on the vertical length of the condensing film. Therefore, the whole thermal calculation of the heat transfer across the condenser/modules/heat sinks is made iteratively until the correct active length of the

condenser is obtained. Electrically, the total voltage and power produced will be estimated by calculating the number of active modules, which will be the total number of modules multiplied by the condenser load. An illustration of a possible system implementing this strategy is presented in Fig. 4.

### Evaporator Model

The evaporator model used in the previous work of the authors was a simplified one, assuming constant heat exchanger effectiveness (ratio between absorbed power and maximum absorbable power) calibrated from experimental data.<sup>16</sup> In the present work, the evaporator is fully modelled through empirical correlations suitable for the heat exchanger geometry under consideration (vertical staggered tube bank evaporator with finned surfaces) and boiling correlations for pressurized water in vertical tubes. A MATLAB model was created to evaluate the unsteady one-dimensional heat transfer occurring between the exhaust gases, the tube banks and the boiling water inside the tubes.

The exhaust gas temperature varies logarithmically along the heat exchanger length. Using a mean logarithmic temperature difference between the fluid and the wall allows for the keeping of a 1D heat transfer analysis.<sup>14</sup>

The model uses, as inputs from the engine and driving models, the mass flow rate and temperature

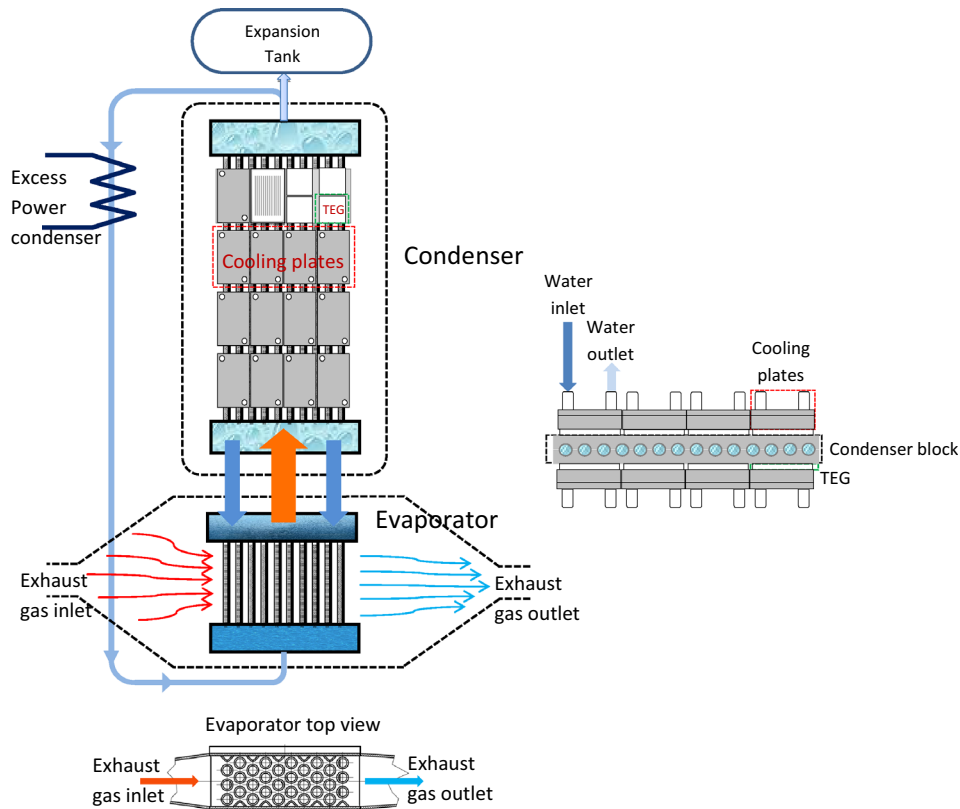


Fig. 4. Outline of the generator concept, with 4 condenser plates and 15 evaporator tubes (reference geometry used in the calculations).

of the exhaust gases to estimate the instantaneous boiling power,  $P_{\text{evap}}$ , at the inside of the evaporator tubes/HPs during the whole driving cycle. To determine this power, it is necessary to solve the unsteady energy equation across the thickness of the pipes with convective and boiling heat transfer at the outer and inner boundaries, respectively.

*Convective Heat Transfer Between Exhaust Gases and Outer Evaporator Wall*

The convection of heat between the exhaust gases and the outer evaporator walls is characterized by an average heat transfer coefficient  $h_{\text{conv}}$ . The heat transfer coefficient for tube banks will depend on the arrangement of the tubes relatively to each other.<sup>14</sup> A staggered tube configuration maximizes heat transfer in comparison with an aligned configuration, so it was chosen for the evaporator design.

The geometric parameters of a staggered tube bank are represented in Fig. 5, with  $S_n$  being the transversal pitch,  $S_p$  the longitudinal pitch and  $D_{\text{ext}}$  the external diameter of the tubes.

The heat transfer in tube bank heat exchangers was extensively studied by researchers such as Grimson<sup>47</sup> and Zukauskas.<sup>48</sup> The latter proposed a correlation to determine the average heat transfer coefficient in tube banks (Eq. 3), which allows a wide range of Reynolds numbers and property variations:

$$h_{\text{conv}} = \frac{k_f C \text{Re}_{d,\text{max}}^n \text{Pr}^{0.36} \left(\frac{\text{Pr}}{\text{Pr}_w}\right)^{1/4}}{D_{\text{ext}}} \times [0.7 < \text{Pr} < 500; 10 < \text{Re}_{d,\text{max}} < 10^6] \quad (3)$$

where  $k_f$  is the fluid thermal conductivity, Pr is the Prandtl number of the gases, and  $\text{Re}_{d,\text{max}}$  is the Reynolds number of the flow based on the maximum velocity achieved at the smallest cross sectional area of the tube banks, while  $C$  and  $n$  are constants

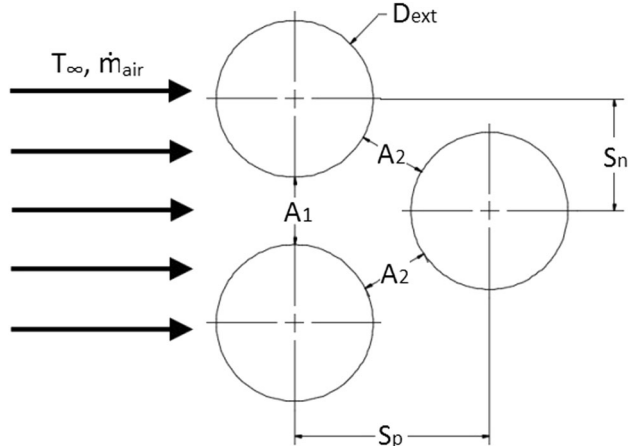


Fig. 5. Tube bank evaporator with staggered arrangement with representation of the tube row pitch and minimum cross-sectional areas.

that depend on  $\text{Re}_{d,\text{max}}$  and on geometric parameters (see Table I). By itself, this correlation is only valid for 20 or more longitudinal rows; nevertheless, correction factors have been proposed for tube banks with fewer than 20 rows (see Table II).

All properties are evaluated at the average fluid temperature between exhaust gas heat exchanger inlet and outlet temperatures, namely  $T_{\text{wall\_in}}$  and  $T_{\text{wall\_out}}$ , except  $\text{Pr}_w$ , which is evaluated at the wall temperature.

The maximum velocity at the tube banks  $u_{\text{max}}$  will occur at the minimum section area, which can be either  $A_1$  or  $A_2$  (as represented in Fig. 5). Expressions for determining  $u_{\text{max}}$  can be found in Ref. 17.

To reduce the total convective thermal resistance, the addition of fins has been considered. For calculation effects they will solely affect the total surface area, through the use of the fin efficiency,<sup>17</sup> as seen further ahead.

*Boiling Heat Transfer Inside Evaporator Pipes*

The fluid inside the pipes is considered to boil under the nucleate boiling regime with a constant pool temperature corresponding to the saturation temperature. This means that the inner pressure is considered to be constant, with the pressure stability being provided by adding an expansion tank as part of the system.

The heat transfer coefficient,  $h_{\text{boils}}$ , for pressurized water boiling inside vertical tubes proposed by Jakob<sup>49</sup> seems rather suitable for the application under analysis (Eq. 4):

$$h_{\text{boil}} = 2.54(T_{\text{wall\_in}} - T_{\text{HP}})^3 \cdot e^{p/1.551}; \times [0.5\text{MPa} < p < 17\text{MPa}], \quad (4)$$

where  $p$  is the pressure inside the tubes, expressed in MPa,  $T_{\text{wall\_in}}$  is the inner pipe wall surface temperature (the wall which is in contact with the boiling bath) and  $T_{\text{HP}}$  is the heat pipe/thermosiphon temperature, that is, the saturation temperature of the steam, which is solely dependent on pressure. This calculation must be iterative, since the temperature difference between the inner wall surface and the boiling temperature is itself a function of the heat transfer coefficient.<sup>17</sup>

*Unsteady Heat Transfer Calculations for the Evaporator*

Given the strong variation of the exhaust thermal load during a driving cycle, it is advisable to solve the one-dimensional time-dependent energy equation (Eq. 5), which has the following form<sup>14</sup>:

$$\frac{\partial T}{\partial t} = \alpha \frac{\partial^2 T}{\partial x^2}, \quad (5)$$

with  $x$  being the coordinate along the tube thickness from the outer tube wall in the direction that is normal to the surface of the tubes and  $\alpha$  being the

**Table I. Constants  $C$  and  $n$  used in the Zukauskas correlation for heat transfer in tube banks of 20 rows or more (adapted from Ref. 46)**

Geometry	$Re_{d,max}$	$C$	$n$
Staggered	10–100	0.9	0.4
	100–10 <sup>3</sup>	Treat as individual tubes	
	10 <sup>3</sup> –2 × 10 <sup>5</sup>	0.35 $\left(\frac{S_n}{S_p}\right)^{0.2}$ for $\frac{S_n}{S_p} < 2$	0.60
	10 <sup>3</sup> –2 × 10 <sup>5</sup>	0.40 for $\frac{S_n}{S_p} > 2$	0.60
	> 2 × 10 <sup>5</sup>	0.022	0.84

**Table II. Ratio of  $h_{conv}(N)/h_{conv}(>20)$  for  $N$  longitudinal rows (adapted from Ref. 46)**

$N$	2	3	4	5	6	8	10	16	≥20
Staggered	0.77	0.84	0.89	0.92	0.94	0.97	0.98	99	1.0

thermal diffusivity of the conductive material. This equation is solved within the tube wall thickness and with convection and boiling boundary conditions at the outer and inner surfaces of the tubes, respectively.

The Eq. 5 is discretized in time and space using finite differences.  $m$  is defined as the index of instant  $t$  and  $i$  is the index of a spatial node located at a depth  $x$  from the outer surface of the tubes.  $\Delta t$  and  $\Delta x$  are the time and space steps/subdivisions.

Using the explicit method it is possible to directly calculate the temperature field  $T^{m+1}$  at instant  $(t + \Delta t)$ , by using the temperature field  $T^m$  from the previous instant  $(t)$  and applying the boundary conditions at the nodes corresponding to the tube outer ( $i = 1$ ) and inner ( $i = n$ ) surfaces. Therefore, for an interior wall node ( $1 < i < n$ ), the discretized energy equation reduces to the following finite difference equation using the non-dimensional Fourier (Fo) number<sup>14</sup> (Eq. 6):

$$T_i^{m+1} = Fo(T_{i+1}^m + T_{i-1}^m) + (1 - 2Fo)T_i^m \quad [1 < i < n], \quad (6)$$

The nodes located at the outer ( $i = 1$ ) and inner ( $i = n$ ) surfaces of the HPs will be affected by forced convection and boiling convection boundary conditions, respectively. The temperature for the next time step  $m + 1$  may be calculated through the following derived expressions

$$T_1^{m+1} = 2FoT_2^m + 2FoBi_{conv} \overbrace{\left(T_{air\ average}^m - T_1^m\right)}^{\Delta T_{log}} + (1 - 2Fo)T_1^m \quad (7)$$

$$T_n^{m+1} = 2FoT_{n-1}^m - 2FoBi_{boil}(T_n^m - T_{HP}) + (1 - 2Fo)T_n^m, \quad (8)$$

with Fo and  $Bi_{conv}$  and  $Bi_{boil}$  being the non-dimensional Fourier number, the convection Biot number and the boiling Biot number, respectively.  $\Delta T_{log}$  is the mean logarithmic temperature difference between the exhaust gases and the external wall temperature, with  $T_{air\ average}^m$  being an imaginary average logarithmic temperature, obtained from Eq. 9:

$$\Delta T_{log} = \frac{T_{exhin} - T_{exhout}}{\ln\left(\frac{T_{exhin} - T_{wallout}}{T_{exhout} - T_{wallout}}\right)}; \quad (9)$$

$$T_{exhaverage} = \Delta T_{log} + T_{wallout}$$

It may be seen that no section area is present in Eq. 6 through Eq. 8. The reason is that since the section area is present in all terms of the equation, it may be cancelled if it's constant. In the present case, the section area is clearly not constant because the outer surface of the HPs is finned, displaying a much higher surface area than the inner surface of the HPs. Moreover, the outer tube surface is slightly larger than the inner tube surface. Nevertheless, it is still possible to use these equations by normalizing the heat transfer coefficients with a reference section area,  $A_{avg}$ , common to all the terms of the equation. This enables the elimination of this term as in the case of the uniform cross section heat transfer. For instance, the convective heat transfer coefficient,  $h_{conv}$  is used in conjunction with the outer surface area  $A_{wallout}$  to compute thermal power. But it is possible to express the heat transfer coefficient as a function of a different area, provided that the product  $hA\Delta T$  is kept constant (by definition the heat transfer coefficient is always defined relatively to a given section surface).<sup>14</sup> So the idea is to express all heat transfer coefficients as a function of a reference area,  $A_{avg}$ . For instance, in the case of convection, the corrected heat transfer coefficient,  $h_{conv\ corr}$ , is obtained as follows:

$$h_{\text{conv}} \cdot A_{\text{wallout}} \cdot \Delta T = h_{\text{convcorr}} \cdot A_{\text{avg}} \cdot \Delta T$$

$$\Rightarrow h_{\text{convcorr}} = h_{\text{conv}} \frac{A_{\text{wallout}}}{A_{\text{avg}}} \quad (10)$$

A similar procedure may be applied to all terms of the energy equation so that the section area term may be cancelled from the energy equation. In the present case, it is useful that the reference area should be the average heat transfer area by conduction, so that the conductive and the capacitive terms of the equation may use the same section area and so Eq. 6 through Eq. 8 may be used.

The Fourier and Biot numbers are calculated as follows (Eq. 11):

$$\text{Fo} = \frac{\alpha_{\text{metal}} \Delta t}{(\Delta x)^2}, \quad \text{Bi}_{\text{conv}} = \frac{h_{\text{convcorr}} \Delta x}{k_{\text{metal}}}, \quad (11)$$

$$\text{Bi}_{\text{boil}} = \frac{h_{\text{boilcorr}} \Delta x}{k_{\text{metal}}},$$

where  $\alpha_{\text{metal}}$  and  $k_{\text{metal}}$  are the thermal diffusivity and conductivity of the material of the HPs, respectively.

For stability reasons, the explicit method requires that the following stability criterion be satisfied<sup>14</sup>:

$$\text{Fo}(1 + \text{Bi}) \leq \frac{1}{2} \Rightarrow \Delta t \leq \frac{(\Delta x)^2}{2\alpha(1 + \text{Bi})}. \quad (12)$$

The heat transfer rate released by the gases and absorbed by the external wall of the HPs is given by Eq. 13:

$$P_{\text{wallout}} = h_{\text{conv}} A_{\text{wallout}} \Delta T_{\text{log}} \quad (13)$$

Note that the real area of the external surface,  $A_{\text{wallout}}$ , accounts for the fin area multiplied by its efficiency,<sup>14</sup> as presented in Eq. 14:

$$A_{\text{wallout}} = A_{\text{nofins}} + A_{\text{fins}} \eta_{\text{fin}} \quad (14)$$

where  $A_{\text{nofins}}$  is the total area of the tube not covered by fins (area of the outer perimeter of the pipe between fins),  $A_{\text{fins}}$  the total area of the fins, and  $\eta_{\text{fin}}$  the fin efficiency, which can be calculated from empirical correlations for the specific fin geometry.<sup>17</sup>

Similarly, the heat transfer rate released to the water through boiling is calculated as Eq. 15:

$$P_{\text{evap}} = h_{\text{boil}} A_{\text{wallin}} (T_{\text{wallin}} - T_{\text{HP}}) \quad (15)$$

This is the thermal power released to the HP interior, which will be the relevant one for the condenser. Note that under steady state regime  $P_{\text{evap}}$  will coincide with  $P_{\text{wallout}}$  but it will not be necessarily so in the unsteady regime.

The outlet exhaust gas temperature,  $T_{\text{exh out}}$  will be a function of the thermal power lost by the gases,

$P_{\text{exh}}$ , which is the same as the power absorbed by the evaporator,  $P_{\text{wallout}}$ . Therefore (Eq. 16):

$$T_{\text{exhout}} = T_{\text{exhin}} - \frac{P_{\text{exh}}}{\dot{m}_{\text{exh}} c_{p\text{exh}}} \quad (16)$$

## Condenser/TE Modules Model

The model for the condenser and for the Thermoelectric modules has been presented previously.<sup>16</sup> It is thermally simpler than the evaporator model, as it has been considered to be *quasi-steady-state*, but it includes thermoelectric effects such as diffuse and localized heat sources and sinks due to the Joule and Peltier effects. The use of a *quasi-steady-state* process seems to be fairly justified for several reasons. Firstly, the changes in the thermal input are damped by the thermal inertia of the evaporator, that is, the variability of the thermal power reaching the condenser will be smaller than the variability of the exhaust input power. Secondly, the materials along the active length of the condenser will experience the same hot source temperature and only the materials located in the vicinity of the non-condensable gas/vapour boundary will suffer instant changes in thermal input.

The heat transfer has been modelled in 1D, but the 3D effects have been considered by using conduction shape factors. A global analytical expression for the calculation of the thermal power absorbed by the condenser and the thermal power released to the cooling system was derived. This analytical expression accounts for all the joule heat sources, both localized (e.g. electrical contact resistance) and diffuse (e.g. TE pellet internal resistance). It accounts for localized peltier heat sinks and sources at the junctions, and it account for all thermal resistances including contact resistances in all interfaces.

The power electronics are not considered; that is, matched load conditions are imposed.

## Interaction Evaporator: Condenser

The inner HP pressure/temperature is considered to be constant due to the high volume of the system provided by the expansion tank. This means that the heat sink temperature of the evaporator ( $T_{\text{HP}}$ ) coincides with the heat source temperature of the condenser and will be constant. Under these conditions, the operation of the evaporator will be virtually unaffected by the operation of the condenser (provided there is no liquid dry-out) and it may be calculated independently of the condenser power. The opposite is not true, since the active condenser length will be dependent on the amount of vapour present.

Two different assumptions may be made concerning the calculation of the condenser power. The simplest one is to consider that the condenser load

will be such that it will always instantaneously consume the exact amount of vapour being generated by the evaporator (with the excess being dissipated by an auxiliary condenser, as implemented in Ref. 16). An alternative assumption may allow the possibility of some vapour accumulation (e.g. a vapour buffer), so that if there is excess vapour production (evaporator power higher than condenser power at full load), there will be some vapour accumulation along the inner volume of the system, up to a given maximum of accumulation. This accumulation (accounted for in energy units) will be released and complement the condenser power once the evaporator power drops below full load condenser power. The latter condition would require some pressure variation, which would slightly affect the boiling temperature, but this pressure variation has been neglected in the present work. Both assumptions (with/without accumulation) have been simulated in the present work.

### Driving Cycle Energy Model

The driving cycle model<sup>29,31,32</sup> characterizes the vehicle's energy flows, following a particular route (e.g. driving cycle), being suitable for normalized and real cycles. The normalized or type approval cycles such as the NEDC (short for "New European Driving Cycle") or WLTP (short for "Worldwide Harmonized Light Vehicles Test Procedure" used in the present work) only acknowledge the influence of the vehicle's speed in the resulting energy flows, while the real cycles may be characterized by further variables; namely, road slope and cornering curvature radius, which like air drag, linear rolling resistance and vehicle inertia, also affect the required traction power. This model has already been presented,<sup>31</sup> so only a brief description is made here.

The output of this model is the instantaneous vehicle propulsion power ( $P_{Prop}$ ), which is the traction power at the wheels needed to propel the vehicle at a given instant of the prescribed driving cycle.<sup>29</sup> The engine power ( $P_{ICE}$ ) and the vehicle propulsion power ( $P_{Prop}$ ) can be related by accounting for the transmission losses through the overall transmission efficiency ( $\eta_{transm}$ ), as presented in Eq. 17:

$$P_{ICE} = \frac{P_{Prop}}{\eta_{transm}}. \quad (17)$$

To know the instantaneous engine speed,  $N_{ICE}$ , it is necessary to know the overall transmission ratio,  $i$ , between engine shaft and the car wheels (accounting also for the differential gear ratio):

$$N_{ICE} = i \cdot N_{wheel}. \quad (18)$$

Naturally, the overall transmission ratio will vary according to the gearbox position, and therefore, a

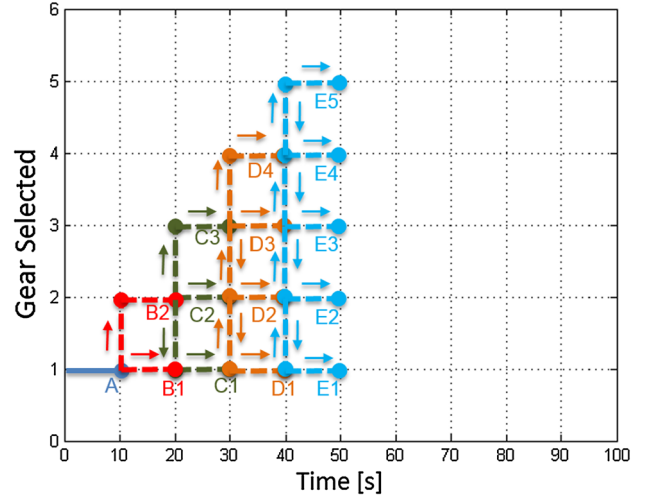


Fig. 6. Graph concept in the shifting gear analysis over time.

realistic gear shifting algorithm must be used.<sup>29</sup> Naturally, the optimum strategy for gear shifting depends on the driver's requirements: maximum power, maximum torque or minimum fuel consumption, resulting in completely distinct optimization processes. An innovative strategy was used by Pires,<sup>29</sup> based on the graph theory, reducing the complexity of the problem to an algorithm based on the search for nearby points in a graph, as depicted in Fig. 6. This strategy has been used by the present work, with the criterion to shift gears based on the engine rotational speed, along with the propulsion power required by the vehicle at a given time.

### SIMULATION CONDITIONS

The generator, thermoelectric modules, vehicle and engine specifications used in the simulations are summarized in Tables III and IV.

#### Generator/Thermoelectric Modules Specifications

##### Vehicle/Engine Specifications

For the simulations a real engine configuration was used, a 1.6 L spark ignition, naturally aspirated, twovalves per cylinder and hemispherical combustion chamber (see details in Table V).

##### Calculated Engine Maps

The torque curves obtained by the engine model for different throttle openings can be seen in Fig. 7. The upper envelope curve corresponds to the maximum brake torque of the engine, obtained for wide open throttle conditions.

The obtained engine maps for exhaust temperature and mass flow rate can be seen in Fig. 8. According to the engine speed and torque (or power, which is torque times the angular velocity) required by the driving cycle model, a unique point in each

**Table III. Evaporator, condenser and cooling plates properties used in the simulations**

<b>Evaporator</b>	
Tube outer diameter (m)	0.014
Tube inner diameter (m)	0.012
Tube height (m)	0.220
Tube material	Stainless steel
Fin thickness (m)	0.001
Fin height (m)	0.001
Fins per mm	0.5
Fin efficiency (%)	99
Tubes per row	3
Tube rows (longitudinally)	10
Sn—Transversal spacing between tubes (m)	0.020
Sp—Longitudinal spacing between tubes (m)	0.0175
P (bar)	46.5
Thp—boiling temperature (°C)	260
(Height × width × length) (m)	0.220 × 0.070 × 0.189
<b>Cooling plates</b>	
Total coolant flow rate (L/h)	2400
Coolant inlet temperature (°C)	25
Cooling plate material	Aluminium
Cooling plate fin length (m)	0.106
Spacing between fins (m)	0.0020
Fin thickness (m)	0.0015
Fin height (m)	0.005
N of fins	16
N of cooling plates	32
Conduction shape factor/cooling plate (m)	4.24
Cooling plate dimensions (length × width × height) (m)	0.1455 × 0.0725 × 0.0100
<b>Condenser</b>	
N of condenser tubes	14
Condenser tubes outer diameter (m)	0.010
Condenser tubes inner diameter (m)	0.008
Condenser plate dimensions height × length × width (m)	0.158 × 250 × 0.015
N of condenser plates	4
Condenser plate shape factor/condenser plate (m)	7.37
Condenser plate material	Aluminium

plot will be identified and used for the thermal algorithm.

### Driving Cycles

**Type Approval Cycles: WLTP Class 3** A standard driving cycle is a normalized schedule that is divided into small time intervals, usually one second, where the acceleration is constant. As a result, the speed varies linearly along the interval, being depicted by a characteristic speed/time diagram. In the present work, one standard cycle has been used: the WLTP Class 3, depicted in Fig. 9. The WLTP test procedure emerged as an effort to create a global standardization procedure for the worldwide comparison of vehicles and as a response to the criticism that the New European Driving Cycle (NEDC) cycle, currently used for the CO<sub>2</sub> and fuel consumption certification of new European vehicles, yielded large discrepancies with real-world vehicle emissions.<sup>35</sup> The WLTP procedure includes three different test cycles representing as many vehicle classes, based upon a vehicle's power-to-mass ratio

(PMR) and its maximum speed.<sup>50</sup> The Class 3 vehicles presents a PMR higher than 34 kW/ton and a top speed above 120 km/h, representing the largest share of modern light-duty vehicles.

**Real Cycles: Highway Cycle (HW)** The selected route connects two cities from the north of Portugal, Guimarães and Braga, via the A11 highway, with a total extension of 27 km completed in 19 min, corresponding to an average velocity of 85 km/h and with a maximum speed of roughly 130 km/h. The altitude profile is steep, with frequent variations along the route and minimum and maximum values of 110 and 320 m. The altitude and speed profile of this driving cycle, along with the most relevant statistical data, are depicted in Fig. 10.<sup>29</sup>

One can still add, regarding the real route cycles, the specific accumulated uphill and downhill parameter, which indicates the positive and negative accumulated altitude variations along the route divided by the route length and thus the route's elevations severity. (in the present case, 17.8 m/km).<sup>29</sup> A

**Table IV. Thermoelectric module properties used in the simulations (ETDYN GM250-49-45-25)**

TEG general data	
General dimensions (length × height × width) (m)	0.620 × 0.620 × 0.0032
Pellet material	Bismuth telluride
Tab material	Copper
Insulator material	Aluminium oxide
N P–N pairs	49
TEG proprieties	
Pellet size (length × height × width) (m)	0.0045 × 0.0045 × 0.0025
Tab size (length × height × width) (m)	0.0105 × 0.0045 × 0.0004
Alumina thickness (m)	0.0008
Contact thermal conductance properties	
$h$ alumina-copper (W/m <sup>2</sup> K)	10250
$h$ copper-Bi <sub>2</sub> Te <sub>3</sub> (W/m <sup>2</sup> K)	10250
$h$ outer surfaces-thermal grease (W/m <sup>2</sup> k)	75000
Conduction shape factor alumina–copper (m <sup>2</sup> /m)	0.0359
Conduction shape factor copper-Bi <sub>2</sub> Te <sub>3</sub> (m <sup>2</sup> /m)	0.0527
Electric resistivity	
$\rho$ copper ( $\Omega$ m)	$1.8 \times 10^{-7}$
$\rho$ contact ( $\Omega$ m <sup>2</sup> )	$1.0 \times 10^{-8}$

**Table V. Reference vehicle and engine specifications used in the simulations**

Vehicle mass (M) (kg)	1400
Tyre rolling resistance coefficient	0.008
Vehicle frontal area (m <sup>2</sup> )	2.22
Drag coef. (Cd)	0.27
Engine type	1.6 L spark ignition, atmospheric, 2 valves/cyl.
Volumetric compression ratio	11:1
Maximum power	88 kW @ 6000 rpm
Maximum torque	160 N m @ 4250 rpm
Redline (rpm)	6500

summary of the HW driving cycle is presented in Table VI.

## RESULTS AND DISCUSSION

Although the engine maps and the driving cycle energy analysis may be properly considered as results of the present analysis, they have been presented in the preceding section as test conditions, since they provide the necessary input (in terms of exhaust temperature and flow rate) for the calculation of the thermal and electrical performance of the thermoelectric generator under study.

Little is said in this paper regarding the thermoelectric model of the modules, but these have been modelled in detail using the same approach presented in previous work,<sup>16</sup> with the Joule and Peltier powers having been accounted for. The Electric Power generated is estimated for the conditions of matched load resistance.

The main parameters analyzed were the thermal and the electric powers within the system. In terms of exhaust inlet thermal power, the available

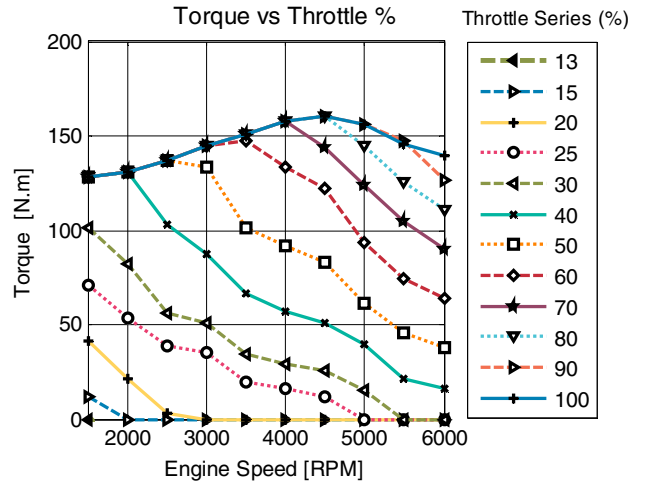


Fig. 7. Predicted engine output torque for different throttle positions and engine speeds.

(absorbable) thermal power entering the heat exchanger was considered. This is the maximum thermal power that could possibly be absorbed by the system, meaning that the chosen reference temperature of the gases corresponding to a zero energy level was the inner HP temperature instead of the ambient temperature, as is often used. In fact, from a second law of thermodynamics perspective, the exhaust gases can only transfer heat to the system as long as they are hotter than the system. The resulting heat transfer effectiveness values presented further ahead are a relative measure of how close the thermal energy absorbed by the condenser was to this theoretical maximum. Of course, using a conventional non-evaporative counter-flow heat exchanger would in theory increase the absorbable heat, since the heat sink temperature would be lower than the HP temperature used

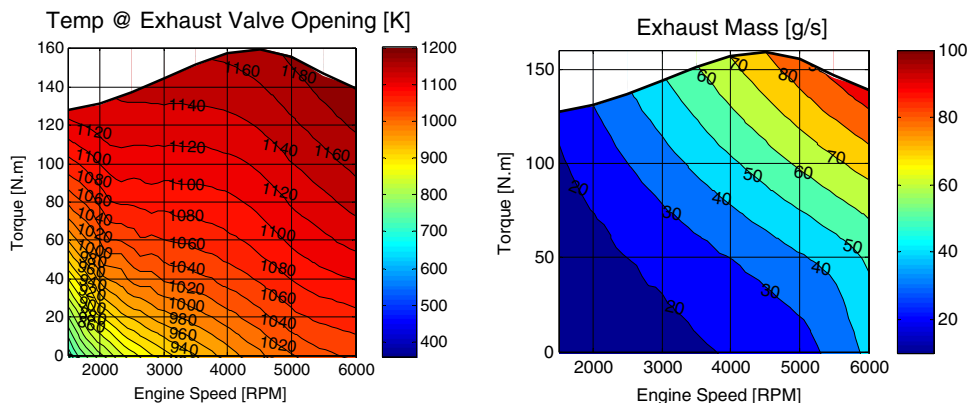


Fig. 8. Predicted exhaust temperature and mass flow rate as a function of engine torque and speed.

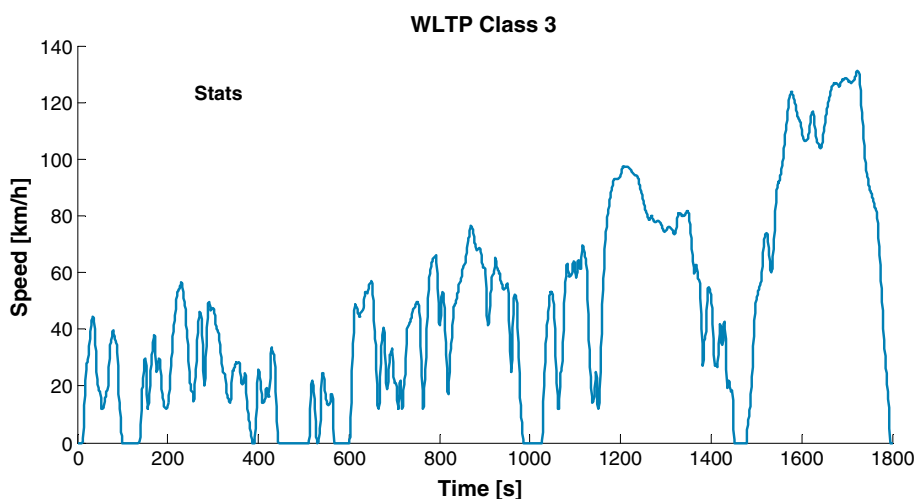


Fig. 9. WLTP Class 3 type-approval cycle.

in this work (260°C). However, the system would lose its ability to control the temperature, so that the hot face temperature is always around its optimum value (around 250°C).

Although a specific generator geometry has been used as a reference for the present analysis, several other evaporator sizes and condenser sizes/TEG module quantities are assessed.

### Reference Generator Geometry Results

Figure 11 displays the temperature profile along all the material layers between the condenser vapour and the cooling circuit. All TE modules located at the active region will sensibly display this temperature profile, as they have roughly the same hot source (vapour) and cold source (water cooling circuit) temperatures. It may be seen that the greatest temperature drop occurs across the TE pellet. This is desirable, since the output depends on this temperature differential. The temperature differences appearing at the other material layers are just deprecating the temperature differential across

the TE pellet, compromising input. The temperature drop due to thermal contact resistance is apparent between the boundaries of each material layer.

Figure 12 highlights the voltage and electric power of the generator as a function of the active condenser length. The deviation of the voltage/electric power curve from linearity is hardly visible, because all active modules experience the same heat source and heat sink temperatures, and because the heat transfer coefficient due to film condensation varies only very slightly with the active length. The cooling occurs in parallel, so there are no differences in average cooling water temperature among the different modules either. Therefore, the output of the system, comprised of the sum of the outputs of active modules is virtually proportional to its active length.

Figures 13 and 14 display the results for the reference generator geometry in terms of available exhaust power (relatively to the HP temperature), evaporator and condenser thermal powers and electrical power generated, for the WLTP Class 3



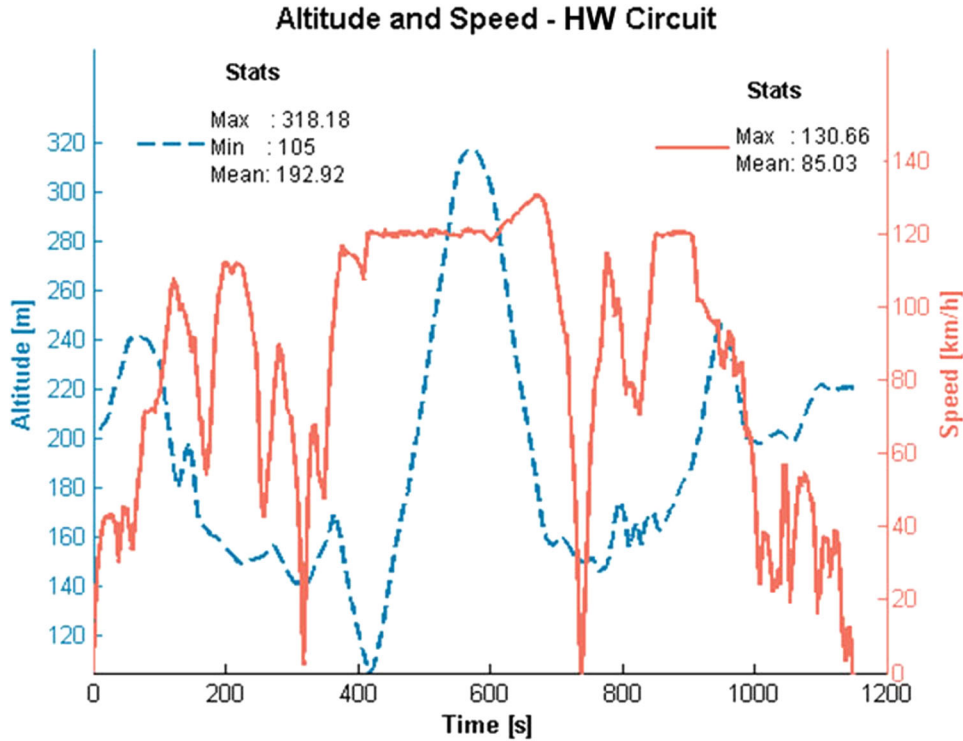


Fig. 10. Custom highway cycle (HW), with non-negligible road slope (adapted from Refs. 23 and 29).

Table VI. Highway route (HW) details

	Highway route	
	Average	Máx.
Engine speed (rpm)	2806	5372
Torque (N m)	65.2	149.1
$P_{ice}$ (kW)	17.1	80.7
Speed (km/h)	85.0	130.6
Throttle (%)	39.5	86.8
Thermal efficiency	0.29	0.34
BSFC (g/kW h)	289	511
T EVO (K)	1096	1186
$\dot{m}_{exh}$ (g/s)	32.07	88.19
$P_{exh}$ (kW)	36.81	111.3

and the real HW driving cycles. This reference geometry (recall Fig. 4) displays  $3 \times 10$  evaporator tubes, a 75 L/h/cooling plate (cooling is performed in parallel), and four condenser blocks with  $2 \times 4 \times 2$  TEG modules per block (64 in total).

The evaporator power,  $P_{evap}$ , (recall Eq. 15), is the instantaneous power being released by the evaporator to the water through boiling. It can be seen that it is generally close to the available power, meaning that the effectiveness of this heat exchanger is high. It can also be seen that there is little influence of the unsteady effects, namely the accumulation of heat within the pipe walls, since no

relevant delay or damping of the evaporator power relative to the input power is apparent. It is true that not all metal masses were incorporated into the analysis (only tube material), but it seems that the system might be suitably treated as *quasi-static*, without the need of using the unsteady analysis at the evaporator.

Since no heat transfer inertia has been considered between the boiling and the condensation phenomena, it can be observed in Figs. 13 and 14 that there is no difference between the condenser power and the evaporator power unless the latter exceeds the condenser's full load power (recall that the load of the condenser varies only according to its active length, not according to the condenser's heat source temperature, which is constant). It may be seen in Fig. 13 that the full condenser capacity was rarely achieved during the low power WLTP driving cycle. The full condenser load may be identified by the thermal power limit of around 15 kW, which corresponds roughly to 900 W of electric power, with all the TE modules being active. During the more severe Highway route (Fig. 14), it may be seen that the condenser was at full load for longer.

The electric power produced is fairly proportional to the condenser power because the temperature levels of the hot source are always the same, with the only variation being the active condenser length. This seems to be another advantage of the system, since the hot side temperature of the active modules is always near the optimum value (the temperature limit of the modules). This

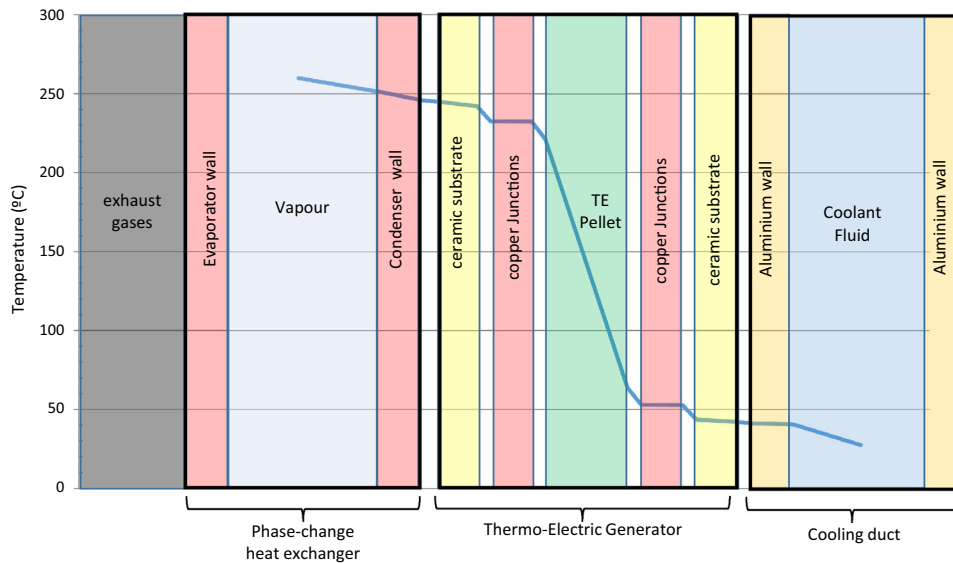


Fig. 11. Temperature profile for a fully active TE module operating at matched load, including thermal contact resistances.

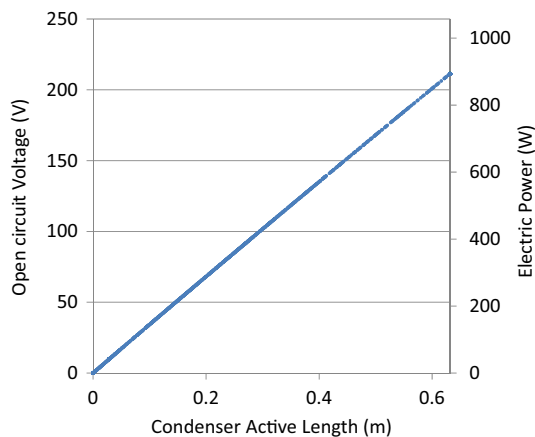


Fig. 12. Open circuit voltage and electric power output as a function of condenser active length.

characteristic may be referred to as “absence of thermal dilution”, because even if the number of condenser plates/modules is high, it will not dilute the temperature at the hot side, because the VCHP operation of the system automatically adjusts its active length to the evaporator power.

### Influence of Allowing for Excess Vapour Accumulation

The incorporation of unsteady thermal effects in the evaporator provided a slight thermal inertia to the system through the heat capacity of the tubes. This is advantageous since it tends to smooth the highest and lowest power events, reducing the situations where the condenser capacity is exceeded or wasted. Some sort of energy accumulation during excess peak events would also be welcome. A phase change device with an expansion tank such as the one proposed in the present work may be suitable for

that purpose. A rough estimation for the geometry under analysis provides a potential of around 150 kJ for boiled vapour accumulation, although some pressure increase will necessarily result (it has been neglected in the present analysis).

In the case of the low power WLTP route, hardly any accumulation could be observed, so the plot is not presented here. In the case of the highway route, there are some differences between the electric production with (w/) or without (w/o) accumulation. It may be observed in Fig. 15 that there is a strong accumulation of vapour during the Highway uphill portion of the driving cycle between 400 s and 600 s. This accumulation achieved the 150 kJ limit at around 450 s, and subsequently allowed for an extension of the full condenser load operation until around 600 s (see decreasing portion of the curve).

### Influence of Evaporator Size

Increasing the size of the evaporator improves the effectiveness of the heat exchanger as a whole, with a higher fraction of the available exhaust heat being captured by the system. But to maximize the output of the system both the evaporator and the condenser should have suitable sizes.

Ideally, the evaporator power capacity should not limit the condenser power capacity. Three different evaporator sizes ( $3 \times 5$ ,  $3 \times 10$  and  $3 \times 15$  tubes) have been assessed, with their thermal and electric powers shown in Figs. 16 and 17 for the HW driving cycle and in Fig. 18 for the electric power generated during the WLTP driving Cycle. It is apparent that the smallest evaporator (the one with  $3 \times 5$  tubes) is clearly too small for the job, even for the lower specific power WLTP cycle. On the other hand, the reference evaporator (the one with  $3 \times 10$  tubes) yields an electric power that is only marginally

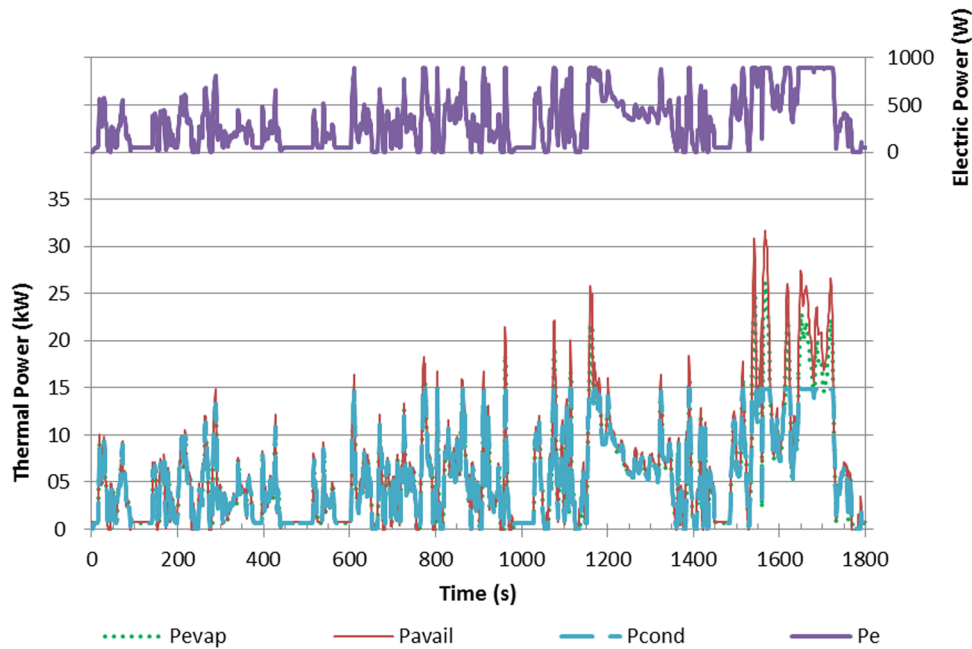


Fig. 13. Reference Generator thermal and electric performance during the WLTP route—available ( $P_{avail}$ ) exhaust power, evaporator ( $P_{evap}$ ) and condenser ( $P_{cond}$ ) thermal powers and electrical ( $P_e$ ) power generated, without vapour accumulation.

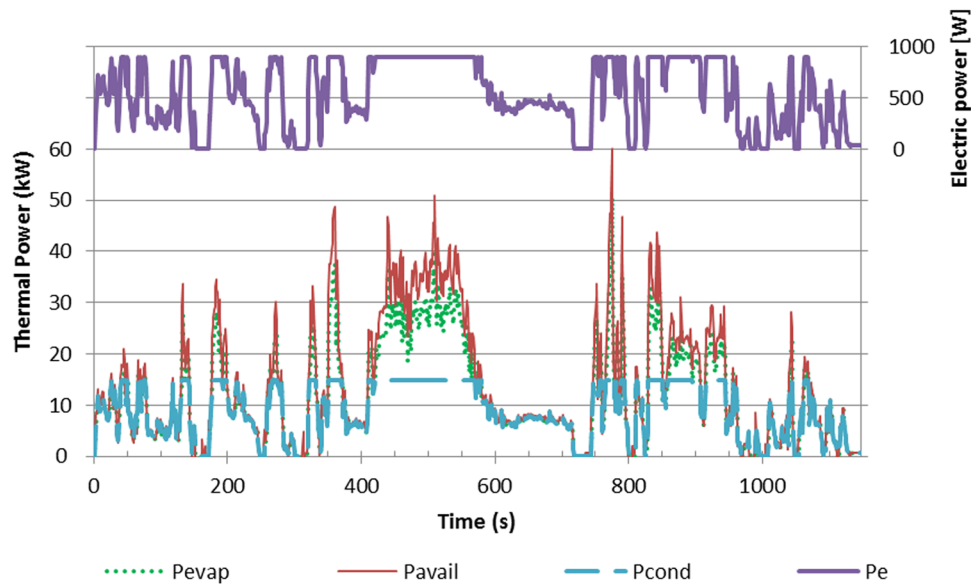


Fig. 14. Reference Generator thermal and electric performance during the HW route—available ( $P_{avail}$ ) exhaust power, evaporator ( $P_{evap}$ ) and condenser ( $P_{cond}$ ) thermal powers and electrical ( $P_e$ ) power generated, without vapour accumulation.

lower than that produced by the biggest evaporator (the one with  $3 \times 15$  tubes), so it seems that the reference geometry would be a good choice for a real application.

### Influence of Condenser Size/Number of Modules

The condenser size is important since it determines the maximum absorbable thermal input, and also because the number of modules is proportional

to the number of condenser plates (16 per plate in the present design, recall Fig. 4). The effect of altering the condenser size is analyzed in Figs. 19 and 20, for the HW and WLTP driving cycles, respectively. There is clearly a power threshold for a given condenser size, which coincides with the maximum condenser capacity. It is clear from Fig. 20 that in the WLTP, the biggest condenser improves the performance of the system only for a few test conditions. The effect of vapour

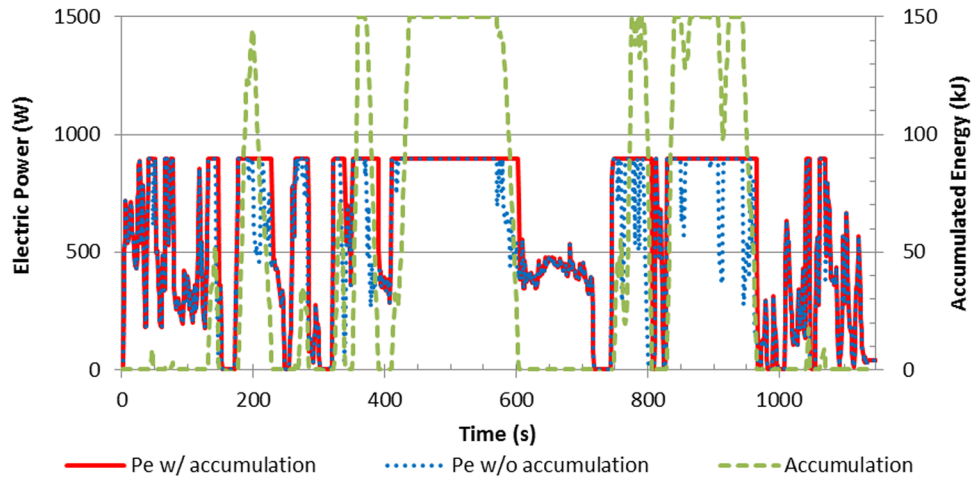


Fig. 15. Effect of vapour accumulation on the electric power produced by the generator during the Highway route.

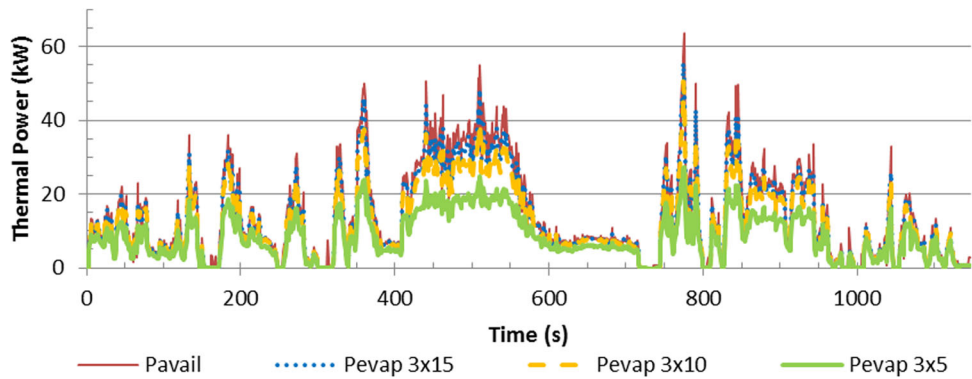


Fig. 16. Influence of evaporator size on boiling power in the Highway driving cycle.

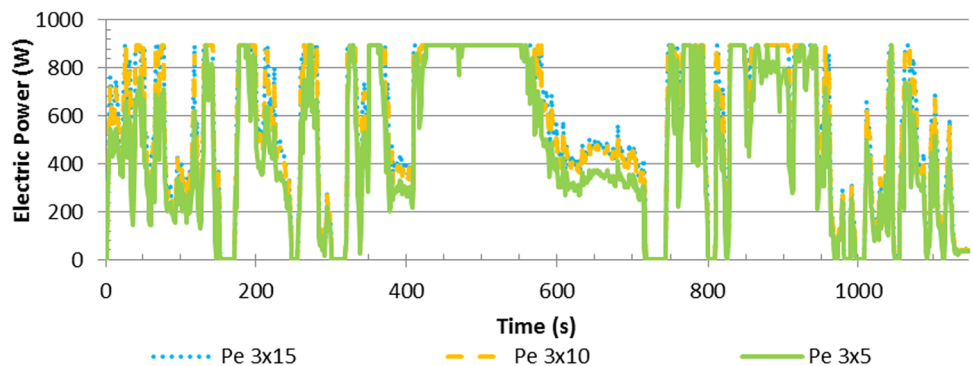


Fig. 17. Influence of evaporator size on electric power in the Highway driving cycle.

accumulation is not shown here, but it will improve the output especially in the case of smaller condensers, where the excess power will be higher (recall Fig. 15).

### Global Exhaust Heat Exchanger Effectiveness

The global effectiveness of the heat transfer from the exhaust to the modules may be seen in Fig. 21 for the Highway and WLTP driving cycles, for all

combinations of evaporator and condenser dimensions, with and without vapour accumulation. The meaning of this effectiveness is the ratio of the absorbable exhaust power that effectively reached the modules. It is a measure of the thermal performance of the system, the fraction of exhaust energy that was successfully directed towards the modules. It may be seen that the global heat exchanger effectiveness increases as the evaporator and the

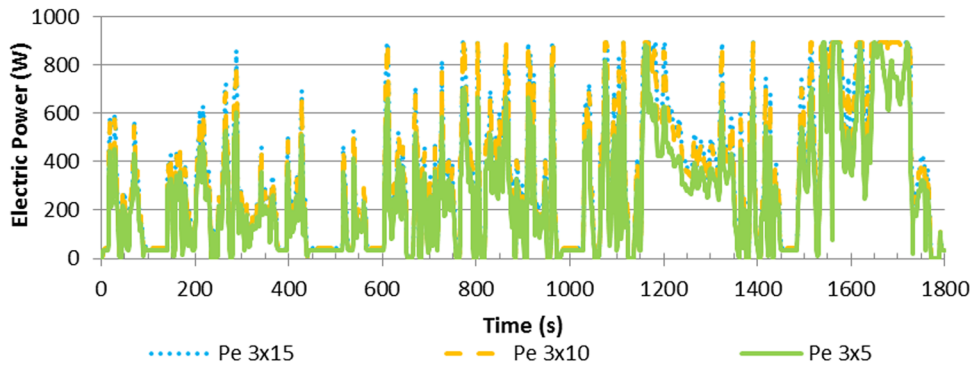


Fig. 18. Influence of evaporator size on electric power in the WLTP driving cycle.

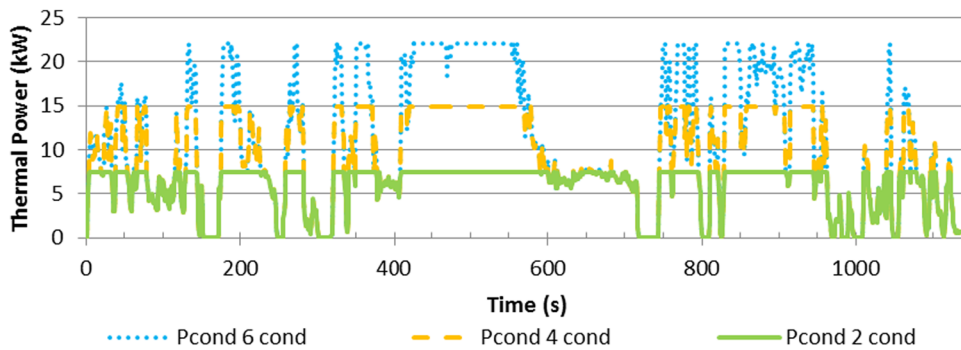


Fig. 19. Influence of condenser size over the thermal power absorbed by the condensers, in the Highway driving cycle.

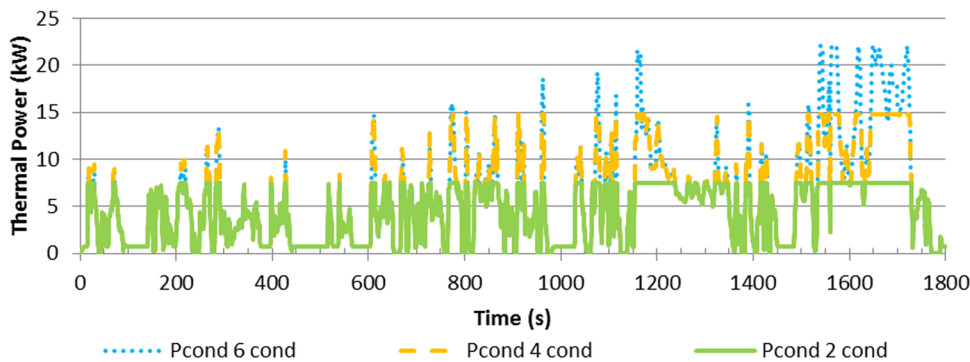


Fig. 20. Influence of condenser size over the thermal power absorbed by the condensers, in the WLTP driving cycle.

condenser get bigger or the accumulation is higher. However, it may be observed that the increase of the condenser size will have a small or even negligible impact on the effectiveness in the cases where the evaporator power is already limited. This happens when the evaporator is small (15 tubes), and in the case of the low specific power WLTP driving cycle, where increasing the condenser from four to six plates hardly increases effectiveness.

### Influence of Coolant Flow Rate

Another small factor affecting power output is the coolant flow rate, as it affects the ability of the modules to maintain a low temperature at the cold

junction of the modules. If this thermal power is not suitably dissipated at the cold face of the module, the temperature differential across the hot and cold junctions of the modules will be depreciated. Nonetheless, increased pumping power will also depreciate the net electric output of the system, so trade-offs of the combination of these effects should be assessed in a real system.

In the present work the cooling flow has been considered to occur in parallel over the cooling plates, with each cooling plate serving two TEG modules (recall Fig. 4). Figure 22 displays the influence of cooling flow rate on electric output (pumping power has not been included). It can be seen that an

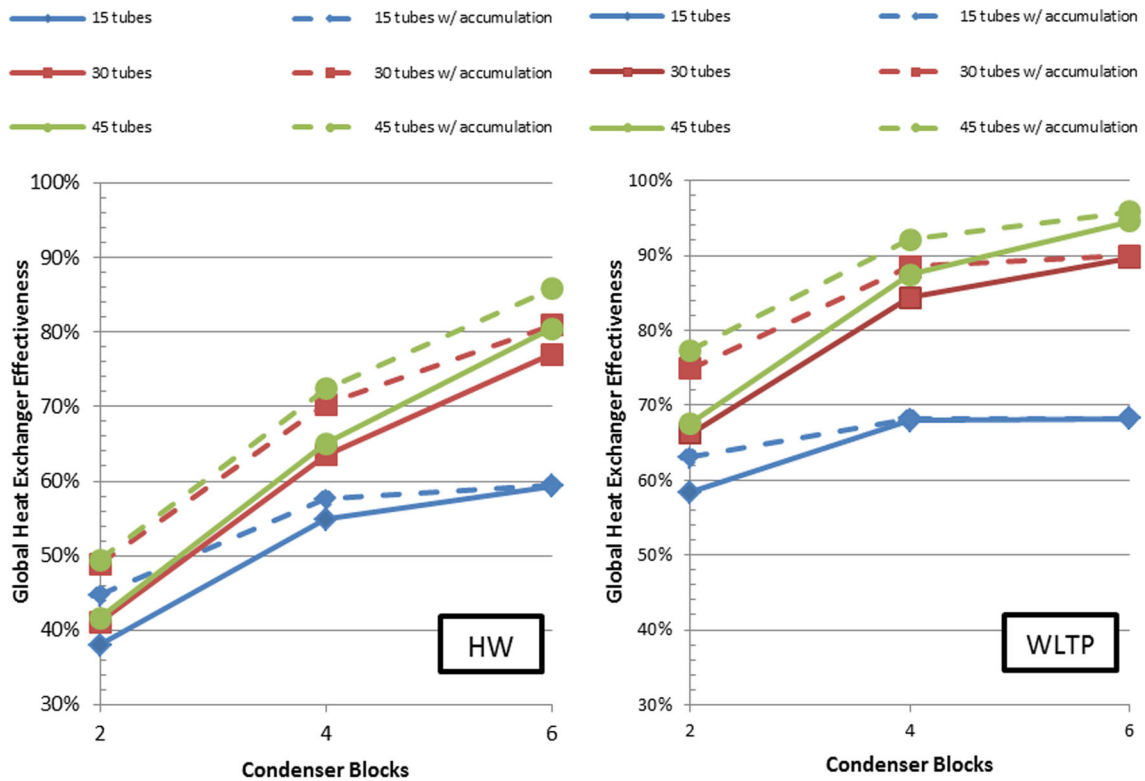


Fig. 21. Global Heat Exchanger Effectiveness during the (a) Highway and (b) the WLTP driving cycle.

increase in electric output between 3.5% and 5% is obtained when doubling the flow rate from 50 L/h to 100 L/h. It is likely that this increase might not be sufficient to compensate for the extra pumping power required to double the flow rate.

The last two charts of this paper (Figs. 23 and 24) provide an overview of the thermal and electric power figures resulting from all combinations of evaporator and condenser sizes, with and without vapour accumulation, for both the Highway and the WLTP Class 3 driving cycles.

The first point that may be taken from these charts is that the HW and the WLTP driving cycles display totally different thermal and electric power levels, denoting diverse average vehicle specific powers (VSPs).<sup>32</sup> As would be expected, an increase of evaporator and condenser sizes tends to increase these powers. Nevertheless, it may be seen that when increasing the condenser capacity from four to six condenser plates in the case of the WLTP driving cycle, the thermal and electric powers no longer increase. This is because most of the evaporator thermal power is already absorbed with the smaller condenser. Therefore, there is no point in increasing the condenser capacity further under these conditions. In the case of the higher VSP highway driving cycle, increased condenser capacity is still able to somewhat improve the thermal and electric powers, except in the case of the smaller evaporator (15 pipes), where insufficient vapour is generated to activate the extra condenser area.

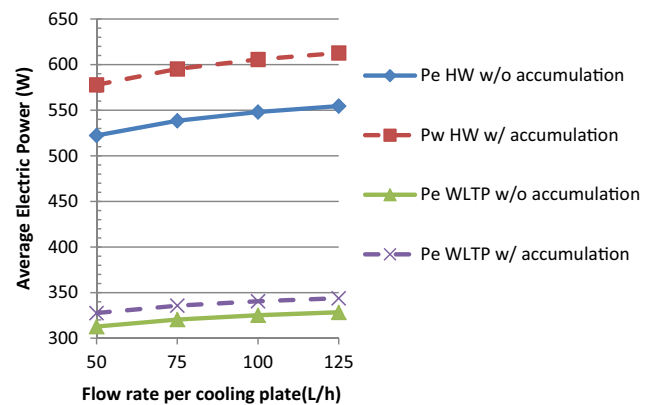


Fig. 22. Influence of coolant flow rate in electric power of the modules.

Regarding the increase of the evaporator size, it has already been noted (recall Fig. 21) that there is no point in increasing it beyond a certain size, because the evaporator effectiveness is already so high that further increasing the evaporator size will only provide a marginal improvement of the thermal power. For instance, it can be seen in Fig. 24 that in the WLTP driving cycle, the electric power increases only 7% when increasing the evaporator 50% in size, from 30 to 45 tubes.

The analysis of the effect of vapour accumulation is also worthy of mention. This vapour accumulation somewhat compensates for the lack of sufficient

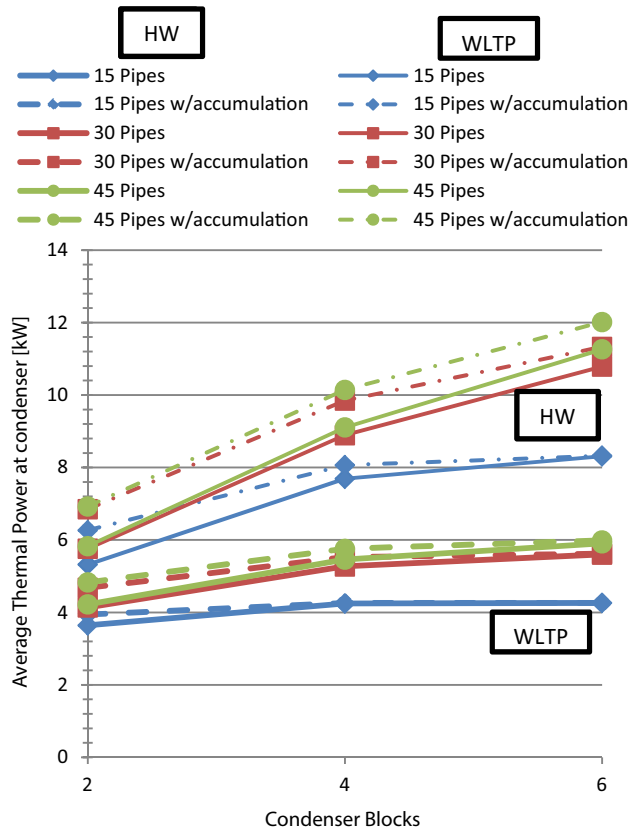


Fig. 23. Average thermal power at condenser as a function of evaporator and condenser size, with and without vapour accumulation.

condenser capacity for the smaller condensers, avoiding the complete waste of the excess vapour produced. This vapour cannot be instantaneously absorbed by the condenser, but may be partially stored within the system and then condensed once the evaporated power drops below the full load condenser power.

As a final remark, it is worth noting that the 320 W (350 W w/accumulation) and 550 W (600 W w/accumulation) produced by the reference system for the WLTP and HW driving cycles seem rather good power figures for a small engine hatchback car such as the one considered in the present analysis and using off-the-shelf Bismuth Telluride modules. These predicted values are of the same order of magnitude of the powers obtained by OEM-backed projects using much bigger vehicles.<sup>11,12,13</sup>

## CONCLUSIONS

An overall model for the assessment of a temperature-controlled automotive exhaust heat thermoelectric generator, operating during driving cycles has been presented. This model incorporates several sub-models, namely those related to engine performance prediction and energy assessment of driving cycles, as well as a unsteady heat transfer model for an exhaust heat exchanger based on phase change

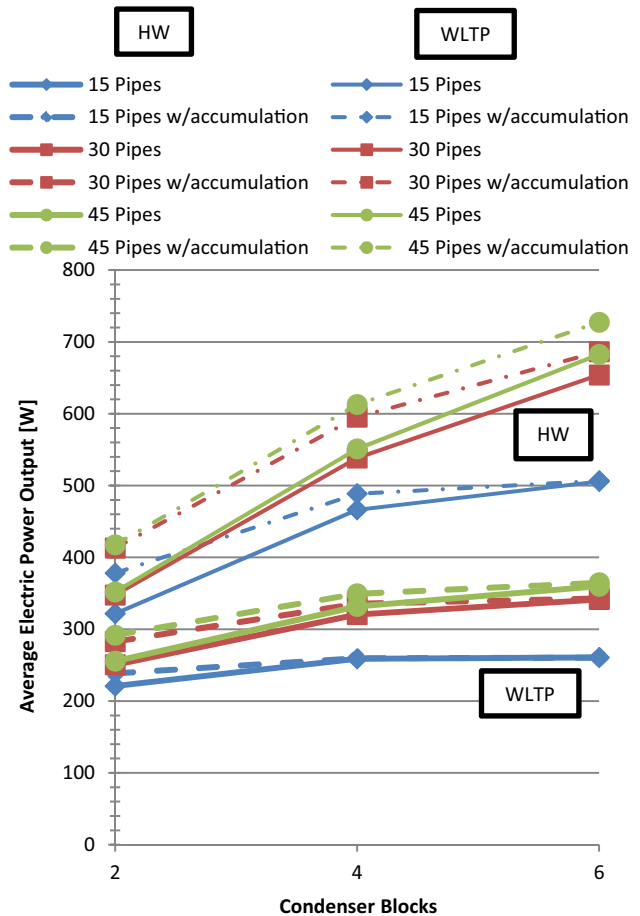


Fig. 24. Average electric power at condenser as a function of evaporator and condenser size, with and without vapour accumulation.

and a model for predicting the behaviour of thermoelectric modules presented in a previous publication.

The engine model for the 1.6 L spark ignition engine was able to predict the full engine performance maps and exhaust flow maps. The driving cycle model used this information for calculating the instantaneous engine conditions along a Type-Approval driving cycle (WLTP Class 3) and a real HW driving cycle. The thermal and electric models of the generator were used to estimate the instantaneous thermal and electric powers of the system during those driving cycles.

It was found that the combination of evaporator and condenser sizes is important for the optimization of the generator output. As expected, the severity of the driving cycle strongly impacts the cycle-averaged TE electrical power output. For the baseline configuration, with 30 evaporator tubes and four condenser blocks, the average electrical power outputs were approximately 320 W and 550 W for the WLTP and HW driving cycles, respectively. For this particular configuration, adding accumulation via vapour storage increased

average electric power by less than 5% and was found to contribute more for severe drive cycles. The possibility of accumulating some of the excess vapour production proved to be especially useful for smaller systems, however.

The merit of the proposed generator concept was confirmed in the sense that it was possible to attain an optimized operation under broadly variable engine loads without the risk of module overheating or thermal dilution. In fact, the main feature of the generator concept proposed is that it works at a prescribed temperature, with the thermal load being varied by the active condenser/module area and not by temperature variation, as in conventional generators. Therefore, it was possible to utilize most of the available exhaust heat with the active modules always operating at top efficiency, without thermal dilution or overheating risk. The main challenge of this concept will be to achieve a viable packaging for light vehicles.

### ACKNOWLEDGMENTS

Project ThinHarvest (FCOMP-01-0124-FEDER-041343/EXPL/EMS-ENE/1023/2013) and Post doctoral Grant SFRH/BPD/89553/2012, financed by FEDER funds through Programa Operacional Factores de Competitividade—COMPETE and National funds through PIDDAC and FCT—Fundação para a Ciência e a Tecnologia; Luso-American Foundation/National Science Foundation (FLAD/NSF) 2013 PORTUGAL—U.S. Research Networks Program, Project “Waste Exhaust Energy Recovery of Internal Combustion Engines”; ENERGEST, for the support in the design and construction of the proof-of-concept prototype.

### REFERENCES

- J. Ribau, C. Silva, F.P. Brito, and J. Martins, *Energy Convers. Manage.* 58, 120 (2012).
- J. Martins and F.P. Brito, *Carros Eléctricos* (Porto: Publindustria, 2012).
- B.J. Heywood, *Internal Combustion Engines Fundamentals* (New York: McGraw-Hill, 1988).
- J. Martins, *Motores de Combustão Interna*, 4th ed. (Porto: Publindustria, 2013).
- J. Yang and F.R. Stabler, *J. Electron. Mater.* 38, 7 (2009).
- L. Bell, *Science* 321, 1457 (2008).
- D.M. Rowe and G. Min, *IEE P Sci. Meas. Technol.* 143, 6 (1996).
- M.S. Dresselhaus, G. Chen, M.Y. Tang, R.G. Yang, H. Lee, D.Z. Wang, Z.F. Ren, J.-P. Fleurial, and P. Gogna, *Adv. Mater.* (2007). doi:10.1002/adma.200600527.
- G. Min, and D.M. Rowe, *CRC Handbook of Thermoelectrics*, ed. D.M. Rowe (Boca Raton: CRC Press, 1995), Chapt. 38.
- F.P. Brito, L. Figueiredo, A.P. Cruz, L. Rocha, L.M. Gonçalves, J. Martins, and M. Hall, *J. Electron. Mater.* (2015) doi:10.1007/s11664-015-4182-x.
- J. LaGrandeur, D. Crane, S. Hung, B. Mazar, and A. Eder, *ICT'06* (2006) doi:10.1109/ICT.2006.331220.
- H. Zervos, Waste heat recovery systems in vehicles (Energy Harvesting Journal, 2011), <http://www.energyharvestingjournal.com/articles/waste-heat-recovery-systems-in-vehicles-00003754.asp>. Accessed 11 Nov 2015.
- G.P. Meisner, Skutterudite Thermoelectric Generator For Automotive Waste Heat Recovery (3rd Thermoelectric Applications Workshop, 2012), <http://energy.gov/sites/prod/files/2014/03/f10/meisner.pdf>. Accessed 11 Nov 2015.
- F.P. Incropera, *Fundamentals of Heat and Mass Transfer* (Hoboken: Wiley, 2011).
- D. Reay and P. Kew, *Heat Pipes: Theory, Design and Applications*, 5th edn. (Butterworth-Heinemann: Elsevier, 2006), pp. 66, 67, 81, 215–218.
- F.P. Brito, J. Martins, E. Hançer, N. Antunes, and L.M. Gonçalves, *J. Electron. Mater.* 44, 6 (2015). doi:10.1007/s11664-015-3638-3.
- J.P. Holman, *Heat Transfer* (New York: McGraw-Hill, 2009).
- V. Kumar, S. Saini, M. Sharma, and K.D.P. Nigam, *Chem. Eng. Sci.* 61, 4403 (2006).
- J. Martins, K. Uzunecanu, B. Ribeiro, and O. Jasansky, SAE Technical Paper Series 2004-01-0617 (2004).
- Ricardo plc, What is WAVE. (Ricardo plc, 2015), <http://www.ricardo.com/en-GB/What-we-do/Software/Products/WAVE>. Accessed 11 Nov 2015.
- AVL LIST GmbH, AVL BOOST Combustion and Emissions. (AVL LIST GmbH, 2015), [https://www.avl.com/simulation-solutions-for-construction-equipment/-/asset\\_publisher/gYjUpY19vEA8/content/avl-boost-combustion-and-emissions](https://www.avl.com/simulation-solutions-for-construction-equipment/-/asset_publisher/gYjUpY19vEA8/content/avl-boost-combustion-and-emissions). Accessed 11 Nov 2015.
- FEV Group, FEV Virtual Engine. (FEV Group, 2015), <http://www.fev.com/what-we-do/software/virtual-engine-power-train-dynamics-simulation.html>. Accessed 11 Nov 2015.
- Gamma Technologies, Propulsion systems. (Gamma Technologies, 2015) <https://www.gtisoft.com/gt-suite-applications/propulsion-systems/>. Accessed 11 Nov 2015.
- J.P. Hebert, E. Baydar, and D.B. Carrington, KIVA-4 User's Manual. (Los Alamos National Laboratory, 2011), [http://www.lanl.gov/projects/feynman-center/technologies/software/kiva/KIVA-4-WebManual/kiva4\\_users\\_manual.htm](http://www.lanl.gov/projects/feynman-center/technologies/software/kiva/KIVA-4-WebManual/kiva4_users_manual.htm). Accessed 11 Nov 2015.
- ANSYS Inc., IC Engine System. (ANSYS Inc., 2012), <http://www.ansys.com/Resource+Library/Presentations/Introducing+the+ANSYS+Workbench+IC+Engine+System>. Accessed 11 Nov 2015.
- Convergent Science, Inc., Applications: Internal combustion engines, <http://convergecf.com/applications/internal-combustion-engines/>. Accessed 11 Nov 2015.
- B. Ribeiro and J. Martins, SAE Technical Paper Series No. 2007-01-0261 (2007).
- B. Ribeiro, J. Martins, and A. Nunes, *Int. J. Thermodyn.* 10, 2 (2007).
- J.M. Pires (M.Sc. thesis, University of Minho, 2014).
- A. Ambrozik, W. Danilczyk, and S. Kruczyński, *TEKA Kom. Mot. Energ. Roln.* 6, 5 (2006).
- L.A.S.B. Martins, J.M.O. Brito, A.M.D. Rocha, and J. Martins, *Regenerative Braking Potential and Energy Simulations for a Plug-In Hybrid Electric Vehicle Under Real Driving Conditions*, IMECE2009 (Lake Buena Vista: ASME, 2009), pp. 1–8.
- L.B. Martins, B.J.O. Araujo, J.C.F. Teixeira, F.P. Brito, and J. Martins, *Methodology for the Energy Characterization of Type-Approval and Real-World Driving Cycles for Passenger Vehicles (IMECE2015-53669)*, IMECE '2015 (Houston: ASME, 2015).
- P. Mock, J. German, A. Bandivadekar, and I. Riemersma, *ICCT 2012-2* (2012).
- G. Fontaras and P. Dilara, *Energy Policy* 49, 719 (2012).
- L. Ntziachristos, G. Mellios, D. Tsokolis, M. Keller, S. Hausberger, N.E. Ligterink, and P. Dilara, *Energy Policy* 67, 403 (2014).
- L. Kullingsjö and S. Karlsson, *The Possibility for Energy Regeneration by Electrification in Swedish Car Driving*, EVS27, IEEE (Barcelona, 2013).
- G.P. Blair, *Design and Simulation of Four-Stroke Engines* (Warrendale: SAE, 1999).
- K.J. Patton, R.C. Nitschke, and J.B. Heywood, SAE Technical Paper Ser. No. 890836 (1989).



39. D. Sandoval and J.B. Heywood, SAE Technical Paper Ser. No. 2003-01- 0725 (2003).
40. Y.A. Cengel, M.A. Boles, and M. Kanoğlu, *Thermodynamics: An Engineering Approach, vol. 5* (New York: McGraw-Hill, 2011), p. 445.
41. C.R. Ferguson, *Internal Combustion Engines: Applied Thermosciences* (New York: Wiley, 1985).
42. F. Bonatesta, Premixed Combustion in Spark Ignition Engines and the Influence of Operating Variables (INTECH Open Access Publisher, 2013).
43. J. Martins, F.P. Brito, L.M. Goncalves, and J. Antunes, SAE Technical Paper Ser. No. 2011-01-0315, (2011).
44. F.P. Brito, J. Martins, L.M. Goncalves, and R. Sousa, 37th IEEE C Industrial Electronics Society IECON 2011 (IEEE Xplore, Melbourne, 2011).
45. F.P. Brito, J. Martins, L.M. Goncalves, N. Antunes, D. Sousa, and S.A.E. Int, *J. Passeng. Cars Mech. Syst.* 6, 652 (2013). doi:[10.4271/2013-01-0559](https://doi.org/10.4271/2013-01-0559).
46. F.P. Brito, J. Martins, R. Sousa, L.M. Goncalves, and S.A.E. Int, *J. Passeng. Cars Mech. Syst.* 5, 561 (2012). doi: [10.4271/2012-01-1214](https://doi.org/10.4271/2012-01-1214).
47. E.D. Grimson, *Trans. ASME* 59, 7 (1937).
48. A. Zukauskas, *Adv. Heat Transf* 8, 93 (1972).
49. M. Jakob, *Trans. ASME* 60, 38 (1938).
50. The International Council on Clean Transportation, World-Harmonized Light-Duty Vehicles Test Procedure. (The International Council on Clean Transportation, November 2013). [http://www.springer.com/materials/optical+%26+electronic+materials/journal/11664?detailsPage=pltpci\\_2326326](http://www.springer.com/materials/optical+%26+electronic+materials/journal/11664?detailsPage=pltpci_2326326). Accessed 11 Nov 2015.